Published in final edited form as:
Biomaterials. 2014 September ; 35(28): 8164–8174. doi:10.1016/j.biomaterials.2014.04.090.

Prostate cancer xenografts engineered from 3D precision-porous poly(2-hydroxyethyl methacrylate) hydrogels as models for tumorigenesis and dormancy escape

Thomas J. Long, PhD[1], **Cynthia C. Sprenger, PhD**[2], **Stephen R. Plymate, MD**[2,3], and **Buddy D. Ratner, PhD**[1,*]

[1]Department of Bioengineering, University of Washington, Seattle, Washington

[2]Department of Medicine, University of Washington, Seattle, Washington

[3]Geriatric Research, Education and Clinical Center, Veterans Affairs Puget Sound Health Care System, Seattle, Washington

Abstract

Synthetic biomaterial scaffolds show promise for *in vitro* and *in vivo* 3D cancer models. Tumors engineered in biomaterial scaffolds have shown evidence of being more physiologically relevant than some traditional preclinical model systems, and synthetic biomaterials provide the added benefit of defined and consistent microenvironmental control. Here, we examine sphere-templated poly(2-hydroxyethyl methacrylate) (pHEMA) scaffolds as the basis for engineering xenografts from multiple human prostate cancer cell lines. pHEMA scaffolds seeded and pre-cultured with tumorigenic M12 cells prior to implantation generated tumors in athymic nude mice, demonstrating the ability of the scaffolds to be used as a synthetic vehicle for xenograft generation. pHEMA scaffolds seeded with LNCaP C4-2 cells, which require Matrigel or stromal cell support for tumor formation, were poorly tumorigenic up to twelve weeks after implantation even when Matrigel was infused into the scaffold, demonstrating a lack of necessary pro-tumorigenic signaling within the scaffolds. Finally, M12mac25 cells, which are ordinarily rendered non-tumorigenic through the expression of the tumor suppressor insulin-like growth factor binding protein 7 (IGFBP7), displayed a tumorigenic response when implanted within porous pHEMA scaffolds. These M12mac25 tumors showed a significantly higher macrophage infiltration within the scaffolds driven by the foreign body response to the materials. These findings show the potential for this biomaterials-based model system to be used in the study of prostate cancer tumorigenesis and dormancy escape.

*To whom correspondence should be addressed. Buddy D. Ratner, University of Washington Department of Bioengineering, Box 355061, 3720 15th Ave NE Seattle, WA 98195, (206) 685-1005, Fax: (206) 616-9763, ratner@uweb.engr.washington.edu.

Author Disclosure Statement

The authors confirm that there are no known conflicts of interest associated with this publication and there has been no significant financial support for this work that could have influenced its outcome.

Introduction

Prostate cancer is the most commonly diagnosed form of non-cutaneous cancer and the second leading cause of cancer mortality for men. In 2013 it is estimated that there will be over 230,000 new cases and 29,000 deaths in the United States alone [1]. The odds of developing prostate cancer at some point over the course of a man's life are about one in six [2]. The study of a disease as complex as prostate cancer requires preclinical model systems that accurately capture the heterogeneity of the tumor microenvironment. Tumorigenic events from initiation through metastasis are defined by dynamic signaling between cancer cells, immune cells, fibroblasts, endothelial vessels, and extracellular matrix (ECM) proteins [3][4]. Many current preclinical models used to study basic cancer biology and screen potential drug candidates are limited because they do not provide adequate control over these tumor-microenvironmental interactions. Standard *in vivo* xenograft models primarily consist of subcutaneously injected cells or cells mixed with ECM prior to injection and result in largely homogenous growths derived from one cell line. Matrigel has been used as the gold standard matrix for xenografts in many labs for years. Matrigel, a laminin 111-rich basement membrane formulation derived from mouse sarcoma, can expose cancer cells to exogenous soluble signaling molecules and ECM interactions [5] that may not be representative of their native environment and cannot be specifically identified or managed due to batch variability [6]. In addition, Matrigel contains a number of growth factors and cytokines that may or may not be appropriate for the microenvironment of all malignancies.

Biomaterial scaffolds provide an opportunity to circumvent these issues for the tissue engineering of 3D *in vitro* and *in vivo* preclinical tumor models [7][8][9][10]. Such scaffolds permit a greater degree of control over the tumor microenvironment by allowing manipulation of scaffold architecture, surface chemistry, degradation rate, controlled factor release, and mechanical properties. In addition, it has been well established that cells cultured in three dimensions better reflect *in vivo* behavior than their two dimensional counterparts [11][12][13]. Thus, a tissue engineered tumor construct can re-create more physiologically relevant representations of cell proliferation, signaling, and cell-matrix interactions than many model systems currently in widespread use [14]. Biomaterials that have been used as platforms to generate cancer models include poly(lactide-co-glycolide) [15], poly(lactic acid) [16][17], poly(ethylene glycol) [18][19][20], polyacrylamide [21], alginate [22][23], chitosan [24][25][26], silk [27], and hyaluronic acid [28][29]. In general, studies comparing 3D models derived from biomaterials to 2D cultures from cell lines across a range of cancer types have demonstrated *in vitro* proliferation rates closer to those measured *in vivo* [15][25], enhanced drug resistance [15][17][23][25][30], and differential gene expression most notably in the form of upregulated angiogenic factors [15][24][25] [31]. In addition, when seeded biomaterials are implanted *in vivo*, xenografts have displayed accelerated tumor growth and higher vascularization [15][25][28].

The studies described here utilize sphere-templated poly(2-hydroxyethyl methacrylate) (pHEMA) hydrogels as scaffolds for *in vivo* prostate cancer xenografts. pHEMA was selected due to its long history for implant biomaterial applications. Sphere-templating fabrication generates a network of interconnected spherical pores with uniform size displaying an inverted colloidal crystal geometry. The foreign body response to these

materials after implantation has been shown to be pore size-dependent [32][33]. As part of that response, macrophages, endothelial cells, and fibroblasts are recruited to the scaffold pores and generate a more complex microenvironment than is attainable through most *in vitro* or more basic *in vivo* systems with the added potential benefit of microenvironmental adaptability through scaffold modification.

The following studies detail the implantation of sphere-templated pHEMA hydrogels seeded with human prostate cancer cell lines. M12 cells are SV40 large T antigen (SV40T)-immortalized, highly tumorigenic prostate epithelial cells derived from P69 cells. P69 cells are largely non-tumorigenic prostate epithelial cells that serve as a negative control for M12 tumor growth [34]. M12 cells do not require Matrigel to form subcutaneous tumors, so these cells were chosen to confirm that sphere-templated pHEMA scaffolds can be used as vehicles for xenograft generation and to determine if there are differences in tumor growth rates or vascularity when cells are pre-cultured and implanted within porous pHEMA scaffolds. LNCaP C4-2 cells are an androgen-independent, metastatic sub-line of LNCaP prostate carcinoma cells that are largely non-tumorigenic when injected subcutaneously [35][36]. However, LNCaP C4-2 cells become tumorigenic in the subcutaneous space when mixed and injected with an exogenous matrix such as Matrigel, so the rationale for the use of this cell line in a biomaterials-based model is to determine if a synthetic scaffold could be used in place of the natural matrix. Finally, M12mac25 cells are M12 cells that have been transfected with the mac25 gene, which codes for insulin-like growth factor binding protein 7 (IGFBP7), also known as insulin-like growth factor binding protein related protein 1 (IGFBP-rp1). IGFBP7 has been demonstrated to be a potential tumor suppressor in breast [37][38], liver [39], bladder [40], skin [41], and prostate cancers [42][43][44]. The mac25 gene confers a senescence-associated gene expression profile and renders the M12mac25 line quiescent upon implantation with or without Matrigel and can be considered a model system for cancer cell dormancy [45]. Prostate cancer dormancy and the mechanisms of dormancy escape are not well understood and present significant clinical challenges [46][47][48][49]. It has been shown that a majority of prostate cancer patients have disseminated tumor cells present in their bone marrow at the time of primary treatment, but less than 30% of those patients developed recurrent disease 5–15+ years post-initial treatment [50]. Despite its clinical relevance, few mouse models of prostate cancer dormancy currently exist. Here, M12mac25 cells seeded within porous pHEMA scaffolds will be presented as a potential model system to study release from dormancy.

Materials and Methods

Scaffold Fabrication

Sphere-templated pHEMA and poly(2-hydroxyethyl methacrylate-co-methacrylic acid) (pHEMA-co-MAA) scaffolds were prepared as previously described [51]. Briefly, spherical poly(methyl methacrylate) beads (Kupa, Inc.) with a size distribution of 74–86 μm were packed into a glass mold, sonicated, and sintered at 140 °C for 22 hours (pHEMA) or 24 hours (pHEMA and pHEMA-co-MAA). Pore size and sintering time were optimized for cell seeding and culture [51]. Monomer mixtures were photopolymerized around the sintered particles and then washed with dichloromethane to remove the particles and leave a polymer

network of interconnected spherical pores with uniform size. The monomer mixture for pHEMA scaffolds contained collagen I (BD), which was embedded into the polymer. The monomer mixture for the pHEMA-co-MAA scaffolds excluded collagen I and included 5% mol methacrylic acid/mol HEMA. Methacrylic acid was incorporated to add carboxylic acid groups for protein conjugation. The polymer scaffolds were sterilized with 70% ethanol and rehydrated in phosphate buffered saline.

Scanning Electron Microscopy

Scanning electron microscopy (SEM) was performed at the University of Washington Nanotech User Facility. Scaffolds were frozen, lyophilized, and gold sputter-coated before observation on an FEI Sirion scanning electron microscopy.

pHEMA-co-MAA Scaffold Surface-Modification

pHEMA-co-MAA scaffolds were surface-modified by collagen I conjugation using N-(2-dimethylaminopropyl)-N’-ethylcarbodiimide hydrochloride (EDC, Sigma)/N-hydroxysuccinimide (NHS, Covachem) chemistry. Scaffolds were first equilibrated in ethanol, then reacted in a solution of 0.1 M EDC/0.2 M NHS in ethanol for 1 hour at room temperature. Scaffolds were then rinsed with ethanol and incubated with a 100 μg/mL solution of collagen I in ethanol for 30 minutes at room temperature. Protein solutions were removed and replaced with fresh proteins at the same concentration for an overnight incubation at 4 °C. Scaffolds for cell seeding were sterilized in 70% ethanol and re-hydrated to PBS. Scaffolds for surface analysis were washed 5× in DI H2O and vacuum-dried.

Scaffold Surface Analysis

X-ray photoelectron spectroscopy (XPS) was performed on pHEMA-co-MAA samples by the National ESCA and Surface Analysis Center for Biomedical Problems (NESAC/BIO) center at the University of Washington. Triplicate samples of dried pHEMA-co-MAA, pHEMA-co-MAA + EDC/NHS, pHEMA-co-MAA + adsorbed collagen I (no EDC/NHS), and pHEMA-co-MAA + EDC/NHS + collagen I were analyzed by XPS using three spots per sample. Atomic percent carbon, oxygen, and nitrogen on the sample surfaces were calculated and percent nitrogen was used to confirm protein surface conjugation.

M12, P69, and M12mac25 Cell Culture

M12pc (plasmid control, hereafter referred to as M12), P69, and M12mac25 cells were cultured in RMPI complete media [51] (Cellgro). Rehydrated pHEMA scaffolds that were sintered for 22 hours were punched into 6 mm discs and soaked in media for 1 hour at 37 °C prior to cell seeding, which was performed using capillary force as previously described [51]. 50 μL of a 1×10^7 cell suspension was twice applied to the scaffold. The same process was used for seeding scaffolds with concentrated Matrigel (BD), with the cell suspension mixed 1:1 by volume with Matrigel at 4 °C while holding the total cell number applied to each scaffold constant at 1×10^6 cells. Seeded scaffolds were cultured in 24 well plates as previously described [51]. Culture media was replaced every two days. Scaffolds containing cells were cultured for five days prior to implantation. The five day time point was chosen to limit *in vitro* necrotic zone formation and so that scaffolds contained 1×10^6 cells after 3D

culture to match the number of cells being injected with Matrigel [51]. *In vitro* cell proliferation analysis was performed using a previously described PicoGreen® DNA assay [51].

LNCaP C4-2 Cell Culture

LNCaP C4-2 cells were cultured in RPMI 1640 containing 10% FBS, L-glutamine, 1% sodium pyruvate, and 1% antibiotic/antimycotic. Rehydrated 24 hour-sintered pHEMA and pHEMA-co-MAA scaffolds surface-modified with collagen I were punched into 8 mm discs and soaked in media for 1 hour at 37 °C prior to cell seeding. 50 μL of a 2×10^7 cell suspension was twice applied to the scaffold. Seeded scaffolds were cultured in 24 well plates as previously described [51]. Culture media was replaced every two days. Scaffolds containing cells were cultured for seven days prior to implantation. The seven day time point was chosen so that scaffolds contained 2×10^6 cells after 3D culture to match the number of cells being injected with Matrigel [51]. *In vitro* cell proliferation analysis was performed using a previously described PicoGreen® DNA assay [51].

M12 and P69 *In Vivo* Study

All animal experiments were approved by the University of Washington Animal Care and Use Committee (IACUC) and followed federal guidelines for laboratory animal use. Scaffolds were evaluated for cytotoxicity and the presence of endotoxin using standard USP guidelines and the LAL gel clot method, respectively. Seven-week-old athymic nude mice (Harlan) were anesthetized using 2% isofluorane. pHEMA scaffolds were implanted subcutaneously in the right dorsal flank. For mice with cells but without scaffolds, 200 μL of a 1:1 mixture of Matrigel and 1×10^6 cells were subcutaneously injected. Tumor volume (V) was measured using the equation $V = (L\times W^2)/2$, where length and width were determined with calipers. Scaffolds/tumors from two mice in each group were removed after three weeks for preliminary analysis and the rest of the mice were allowed to reach a tumor volume-based study endpoint of twelve weeks. Half of each explant was embedded in OCT and stored at −20 °C for cryosectioning while the other half was fixed in either zinc fixative overnight at 4 °C. The following groups of mice were used for the M12 and P69 cell line studies: M12 + Matrigel (n=6), M12 + pHEMA (n=6), M12 + pHEMA + Matrigel (n=6), P69 + Matrigel (n=5), P69 + pHEMA (n=5), P69 + pHEMA + Matrigel (n=5), pHEMA no cell control (n=6), pHEMA + Matrigel no cell control (n=6).

M12mac25 *In Vivo* Studies

The following groups of mice were used for an M12mac25 cell line pilot study: M12mac25 + Matrigel (n=5), M12mac25 + pHEMA (n=6), M12mac25 + pHEMA + Matrigel (n=5). Tumor volume was measured over twelve weeks, at which point explants were zinc-fixed overnight at 4 °C. A second animal study was run to ensure reproducibility of the M12mac25 results from the pilot study. Six additional athymic nude mice were injected with M12mac25 cells + Matrigel or implanted with pHEMA seeded with M12mac25 cells as described. One mouse was sacrificed from the M12mac25 pHEMA group at D21 for histological analysis while the rest of the M12mac25 explants were removed and snap frozen after twelve weeks for RNA and protein extraction. In total between the pilot and

follow-up studies, nine mice were analyzed at the twelve week endpoint for the pHEMA + M12mac25 and M12mac25 + Matrigel experimental groups. To compare vascularity after three weeks, additional groups of three mice (with two injections or implants per mouse) were either injected with M12mac25 cells + Matrigel or implanted with pHEMA seeded with M12mac25 cells. Mice were sacrificed after D21 and explants were zinc fixed overnight at 4 °C.

LNCaP C4-2 *In Vivo* Studies

The following groups of mice were used for a LNCaP C4-2 cell line pilot study: LNCaP C4-2 + Matrigel (n=6), LNCaP C4-2 + pHEMA (n=6), LNCaP C4-2 + pHEMA + Matrigel (n=6). Scaffolds/tumors from two mice in each group were removed after three weeks for preliminary analysis and the rest of the mice were allowed to reach a tumor volume-based study endpoint of seven weeks. Explants were zinc-fixed overnight at 4 °C for histological analysis. An additional animal study was run to determine whether scaffold surface modifications could allow for LNCaP C4-2 cells to grow tumors in the absence of Matrigel. Groups of six pHEMA or pHEMA-co-MAA + conjugated collagen I scaffolds with seeded and cultured LNCaP C4-2 cells were implanted into athymic nude mice. One mouse with sacrificed from each group at D21 for histological analysis while the rest of the explants were removed and zinc-fixed after twelve weeks.

Histological Analysis

Fixed explants were dehydrated in ethanol and cleared with xylene prior to paraffin embedding. The embedded scaffolds were sectioned with a Leica microtome, and sections were heated at 53 °C for 30 minutes prior to xylene deparaffinization and rehydration through a graded ethanol series. Slides were stained with a standard Masson's trichrome protocol to analyze basic tissue morphology and imaged on a Nikon E800 microscope equipped with Metamorph software (version 6.0, Molecular Devices). Low magnification trichrome images were stitched together into mosaics using Adobe Photoshop software. For immunohistochemical analysis, sections were washed in tris buffered saline (TBS) and endogenous peroxidases were blocked in a 3% hydrogen peroxide solution in TBS. Antigen retrieval was performed using heated 0.01 M pH 6 citrate buffer. After cooling, sections were blocked overnight at 4 °C in TBS containing 0.5% tween-20, 4% normal serum (Vector) from the animal in which the secondary antibody was raised and 0.25% immunohistochemical grade bovine serum albumin (Vector). Primary antibodies were incubated for one hour at room temperature unless otherwise indicated, with a concentration-matched isotype negative control section. Secondary antibodies were incubated at room temperature for 30 minutes. A Vectastain ABC kit (Vector) was used along with a DAB kit (Vector) to generate a brown positive stain. All sections were counterstained with hematoxylin before dehydration and slide mounting in Permount (Electron Microscopy Sciences). Using this procedure, paraffin sections were stained for the SV40 large T antigen (SV40T) [1:100 rabbit IgG (Santa Cruz), 1:200 goat anti-rabbit secondary (Vector)], prostate specific antigen [30 min incubation of 1:300 rabbit IgG (Dako), 1:200 goat anti-rabbit secondary], F4/80 [1:100 rat IgG (AbD Serotec), 1:200 rabbit anti-rat (Vector)], mouse endothelial cell antigen (MECA) [1:10 rat IgG (BD), 1:200 rabbit anti-rat (Vector)], and IGFBP7 [1:100 goat IgG (Santa Cruz), 1:200 rabbit anti-goat

(Vector)]. OCT-embedded explants were sectioned with a Leica cryotome and dried overnight prior to fixation in cold acetone for 10 min. Cryosections were immunostained using the same procedure as described without peroxidase blocking and with a fluorescent secondary antibody (1:100 donkey anti-rat alexafluor 594 (Invitrogen)) and Vectashield hard set mounting medium with DAPI (Vector).

Immunohistochemical Vasculature Analysis

The vasculature of M12 cell-derived xenografts was visualized by immunostaining for MECA on cryosections as described. Three sections per explant were stained. A 2× objective lens was used to take low magnification images of two distinct non-necrotic tumor areas away from the edge of the xenograft. Those images were divided digitally into 7×7 grids using Metamorph software. Five individual areas were selected randomly, and those areas were imaged at high magnification using bright field and fluorescence microscopy. For analysis, the percent area stained by MECA was quantified by applying a triangle threshold coupled with automatic de-speckling using FIJI software. This analysis was employed in place of counting lumens per area because extrapolation of the small number of lumens counted per image to the large explant area proved inaccurate. For the quantification of M12mac25-derived xenograft vascularity, three zinc-fixed paraffin embedded sections per explant were stained with MECA and visualized with DAB. Since the xenografts were smaller, one to two 2× low magnification images were taken encompassing the entire explant. These images were divided into grids in Metamorph and all areas were individually imaged at 20×. The number of lumens per area over the entire explant was counted manually. Alternative quantification with percent area stained was not performed because thresholding could not compensate for the non-specific staining of Matrigel using DAB.

Immunohistochemical Macrophage Content Analysis

Macrophage content within three week and twelve week M12mac25 explants was determined using fluorescent F4/80 immunohistochemistry on paraffin sections as described. Three slides per explant were stained. A low magnification 2× image was taken and a 7×7 grid was placed on the image. Five areas were selected randomly and each was imaged at high magnification. All F4/80+ cells were counted manually and the macrophage density was calculated.

RNA/Protein Extraction

RNA and protein were extracted from M12mac25 snap frozen explants. For RNA isolation, tissues were homogenized in 1 mL Trizol reagent (Invitrogen) and RNA was collected following the manufacturer’s protocol. RNA concentration was quantified using A260/280 measurements from a Nanodrop 2000 (Thermo Scientific). Total protein was isolated by homogenizing tissue in 1 mL Mammalian Protein Extraction Reagent (mPER) supplemented with protease inhibitor, phosphatase inhibitor, and EDTA (Thermo Scientific). Protein concentration was quantified using a standard BCA assay (Pierce).

qRT-PCR

RNA was converted to cDNA using the SuperScript First-Strand Synthesis System according to the manufacturer's protocol with random primers (Invitrogen). Relative real-time PCR was then performed using an ABI 7900HT sequence detection system using SYBR GREEN PCR master mix (Applied Biosystems) as follows: stage 1: 50°C for 2 minutes; 95°C for 10 minutes; stage 2 (40–45 cycles): 95°C for 15 seconds; 60°C for 1 minute; 72°C at 20 seconds; stage 3 (dissociation curve): 95°C for 15 seconds; 60°C for 15 seconds; 95°C for 15 seconds. Polymerase chain reaction data were analyzed using Primer Express Software v2.0 (Applied Biosystems). Target mRNA levels were normalized against glyceraldehyde 3-phosphate dehydrogenase (GAPDH) levels. The following primer pairs were used: (1) GAPDH, forward: GAAGGTGAAGGTCGGAGTC; reverse: GAAGATGGTGATGGGATTTC and (2) IGFBP-7 (NM_001553), forward: GCCATCACCCAGGTCAGCAAG; reverse: GGATTCCGATGACCTCACAGCT.

Results

Scaffold Fabrication and Surface Analysis

Figure 1 shows an SEM image of a sphere-templated pHEMA scaffold displaying a network of interconnected spherical pores around 80 μm in diameter. Figure 2 shows an example of an XPS survey spectra of pHEMA-co-MAA scaffolds alone and reacted with EDC/NHS and collagen I. Atomic percent analysis showed nitrogen content on the scaffold surface to be 0 % for pHEMA-co-MAA, 1.7 +/− 0.8 % for pHEMA-co-MAA + EDC/NHS, 2.4 +/− 0.1 % for pHEMA-co-MAA + adsorbed collagen I, and 11.8 +/− 1.7 % for pHEMA-co-MAA + EDC/NHS + collagen I. The spike in surface nitrogen content from zero in the original polymer to over 11% after EDC/NHS + collagen I reaction is strongly supportive of the surface conjugation of collagen I to the pHEMA-co-MAA scaffolds.

M12 and P69 Xenograft Analysis

Previous studies detailed the capacity of these scaffolds to support cancer cell attachment and proliferation during *in vitro* culture [51]. Figure 3 shows growth curves for implanted seeded pHEMA scaffolds and their Matrigel counterparts. Figure 3A shows that the growth kinetics for the M12-seeded pHEMA implants with and without Matrigel are statistically equivalent to the standard Matrigel-based xenograft injections. The tumorigenic M12 cells proliferated outside the scaffold by five to six weeks. Figure 4 shows a cross section of an explanted M12 seeded pHEMA-derived tumor at twelve weeks, where a tumor has grown around the scaffold. As expected, the poorly tumorigenic P69 negative control cell line did not form tumors up to twelve weeks after implantation in any experimental group (see Figure 3B). Twelve week pHEMA explants of M12-derived xenografts show the scaffold in a necrotic core with viable tumor tissue well outside of the scaffold (see Figure 4). Cell debris and matrix proteins are retained within the scaffold at this late time point. However, three week explants provide a better indication of early events in tumor formation where M12 cells are actively involved with cells participating in the foreign body response to the material. After three weeks there is an infiltration of F4/80+ macrophages into the scaffold in the areas complementary to where SV40T+ M12 cells are located (see Figure 5). We have previously observed macrophage infiltration into unseeded implants as part of the natural

foreign body response to these porous materials *in vivo* [33]. In the present study, by three weeks post-implantation, the M12 cells have begun to proliferate outside the scaffold and invade the foreign body capsule around the material. So, not only are the cells seeded within the scaffold exposed to the macrophages that infiltrate within it, but the cells that proliferate out of the scaffold are also exposed to the macrophages present in the capsule. Thus, one of the key microenvironmental differences between the scaffold-derived tumors and those from Matrigel is the potential for more significant macrophage signaling. Because spheretemplated scaffolds have also been shown to induce substantial vascularity [32][33], we tested whether this effect translated to xenografts derived from these materials. Figure 6 shows that the scaffold-derived M12 xenografts seeded with and without Matrigel showed a statistically equivalent vascularity to the standard M12 plus Matrigel xenografts based on percent MECA+ stained area.

M12mac25 Xenograft Analysis

Interestingly, the M12mac25 cells that are non-tumorigenic when injected subcutaneously with or without Matrigel formed tumors when seeded in the pHEMA scaffolds with and without Matrigel (see Figure 3C). Tumors became noticeable approximately eight weeks post-implantation. Figure 7 shows a representative trichrome stain of a D84 M12mac25-seeded pHEMA explant that demonstrates a clear proliferation of cells outside the scaffold that were confirmed as SV40T+ M12mac25 cells using immunohistochemistry (see Figure 8A). However, IHC analysis of D21 M12mac25 + pHEMA explants shows that M12mac25 cells are not significantly occupying the scaffold at this early time point (see Figure 8B). In contrast to the tumors formed within the pHEMA scaffolds, IHC of M12mac25 + Matrigel explant shows SV40T+ human cells to be largely confined to their small Matrigel plug (see Figure 8C). One possible explanation for M12mac25 tumorigenesis is the loss of mac25 expression. RT-PCR showed a decline in mac25 transcript levels from *in vitro* culture in all twelve week explants, likely due to the heterogeneous cell population *in vivo*. However, IGFBP7 mRNA was significantly higher in the pHEMA group compared with the Matrigel no growth group ($p<0.01$) (see Figure 9). These data demonstrate that mac25/IGFBP7 loss is likely not responsible for the observed M12mac25 phenotypic change.

MECA staining showed no statistically significant differences in vascularity between the scaffold and Matrigel-derived explants at three weeks or twelve weeks (see Figure 10). However, a significant increase in F4/80+ macrophage density was observed in the pHEMA-derived explants compared with those from Matrigel at three weeks ($p<0.005$), with average macrophage density still higher in pHEMA at D84 (see Figure 11A). Macrophage density within the scaffolds themselves was noticeably lower at D84 compared to D21, and macrophage density increased around the edges of the Matrigel explants at D84 compared to D21. However, it is notable that D84 macrophage localization differed between the sample groups. Macrophages in the Matrigel samples were present largely around clusters of M12mac25 cells, whereas macrophages in the pHEMA samples were present in close proximity to M12mac25 cells both within the scaffold and in the bulk tumor region (see Figure 11B–D).

LNCaP C4-2 Xenograft Analysis

Figure 3D shows tumor growth curves for the LNCaP C4-2 pilot study. Compared to standard Matrigel xenografts, which grew large tumors quickly, cell-seeded pHEMA scaffolds were unable to be used as the basis for LNCaP C4-2 xenografts over seven weeks even when cells were seeded into pHEMA with Matrigel. For the *in vivo* study comparing pHEMA and pHEMAco- MAA surface conjugated with collagen I, tumors developed over twelve weeks in one out of six mice for each group regardless of scaffold surface modification. Histological examination of explants from both *in vivo* studies using immunohistochemistry for PSA showed that by the seven and twelve week endpoints, exactly half of the explants from each study stained positive for PSA, confirming that LNCaP C4-2 cells were present in some of the scaffolds, but no longer present in some others (see Figure 12A–B). Seven week LNCaP C4-2 + Matrigel tumors stained strongly for PSA as a positive cell line control (see Figure 12C). For scaffold-derived tumors, PSA+ cells grew out of the scaffold into surrounding tissue, and for the scaffolds with no measurable tumor growth any PSA+ cells remained localized within the scaffold itself.

Discussion

In these studies, we have engineered human prostate tumor xenografts in athymic nude mice based on sphere-templated pHEMA scaffolds seeded with human prostate cancer cell lines. M12 cells injected with Matrigel and seeded into pHEMA scaffolds both with and without Matrigel grew tumors at statistically equivalent rates over twelve weeks and showed no significant differences in vascularity. This demonstrates the capacity for porous pHEMA scaffolds to be used as a vehicle for xenograft generation, but because M12 cells are highly tumorigenic, it is not surprising that the microenvironment produced by the scaffolds by *in vivo* cell recruitment or M12 cell 3D pre-culture did not substantially affect tumor growth or vascularity. Kievit, *et al*. also observed that highly malignant C6 glioma cells did not respond significantly to 3D culture within chitosan-alginate scaffolds compared to other cell lines [24], so it is possible that the advantages of biomaterials-based *in vivo* tumor models could be limited in cell lines that display high inherent tumorigenicity.

On the other extreme, cell lines that require the support of Matrigel or stromal cells to grow tumors may require significant scaffold modifications prior to tumorigenesis from synthetic materials. LNCaP C4-2 cells, which fit into this category, grew very large tumors by seven weeks after subcutaneous injection with Matrigel, but were poorly tumorigenic in pHEMA. Surface modification of pHEMA-co-MAA scaffolds with collagen I did not increase tumor development, with only one of six mice developing tumors over twelve weeks. The scaffold microenvironment, possibly mediated by the foreign body response to the porous scaffold, appears to inhibit the pro-tumorigenic signaling provided by Matrigel constituents, as demonstrated by the observation that even LNCaP C4-2 cells seeded into pHEMA with Matrigel did not grow. Importantly, synthetic polymers like pHEMA are adaptable to studies designed to modify the microenvironment in a controlled manner. It is possible to covalently conjugate adhesion proteins such as laminin 111 or collagen IV that are highly enriched in Matrigel or dope the polymer with soluble proteins for sustained release to determine which if any can be used individually or in combination to generate a tumor model without batch

variability contributing to tumor growth. Additionally, sphere-templated materials vascularize in a pore-size dependent manner, with a pore size around 38 μm showing the highest vessel density [32]. Since this study used a pore size of approximately 80 μm *i.e.* optimized for cell seeding [51], it is expected that a significant increase in xenograft vascularity still could be achieved using the optimal pore size, which could enhance malignancy or possibly permit the invasion of cell types that might diminish malignancy.

M12mac25 cells, which express the tumor suppressor IGFBP7, remained largely dormant when injected with Matrigel, but grew tumors when implanted within porous pHEMA with or without Matrigel. RNA analysis demonstrated no loss of mac25 expression in the pHEMA samples that grew tumors relative to the dormant Matrigel samples. Thus, some element of the microenvironment resulting from scaffold implantation, and not mac25 loss, is likely responsible for M12mac25 dormancy escape. Current theories regarding tumor dormancy escape, such as angiogenic release and immunosurveillance evasion [46], likely do not account for these observations. Immunohistochemical analysis showed no significant differences in endothelial vessel density between the pHEMA and Matrigel-derived explants, and athymic nude mice have a compromised adaptive immune system that does not demonstrate T cell-mediated destruction of cancer cells. Alternatively, the foreign body response to implanted biomaterials attracts activated macrophages to the implant site, and it has been established that sphere-templated materials induce substantial macrophage infiltration within their porous network [33]. Indeed, F4/80+ macrophage density was higher in the pHEMA explants at both three and twelve weeks, where at both time points macrophages in pHEMA-derived tumors were present in close proximity to M12mac25 cells as opposed to localized around clusters of M12mac25 cells. It has been well-established that tumor-associated macrophages can activate pro-tumor signaling pathways [52][53], and it is possible that the cell signaling mediated by macrophage interactions plays a significant role in the observed M12mac25 cell re-activation. It is also possible that given the large difference in stiffness between the pHEMA scaffolds and Matrigel, mechanical cues may contribute to changes in cell behavior, something that has been observed in a variety of cell types including cancer cells involved in metastatic progression [54][55][56]. Synthetic biomaterials allow for the modulation of scaffold mechanics, which permits this avenue to be investigated. Future studies will attempt to elucidate the mechanism of M12mac25 senescent cell re-activation following implantation within porous biomaterial scaffolds. If a molecular target can be established, it is conceivable to attempt to maintain cells in a dormant state despite the presence of factors that drive dormancy escape. Biomaterials-based tumor model systems such as the one presented in these studies show the potential to provide unique insight into dormancy and other topics in cancer research by allowing for a more controllable manipulation of the 3D tumor microenvironment.

Conclusions

These studies demonstrate the capacity for sphere-templated pHEMA scaffolds to be used as the basis for generating *in vivo* human prostate cancer xenografts for some cell lines. M12 cells seeded and implanted within porous pHEMA generated tumors with equivalent growth kinetics and vascularity to gold standard Matrigel-based xenografts. LNCaP C4-2 cells did not yield tumors from the scaffolds despite collagen-I surface modification or the presence

of Matrigel, indicating a lack of necessary pro-tumorigenic signaling within the scaffolds. Dormant M12mac25 cells re-activated to form tumors from the scaffolds, and explants showed significant macrophage infiltration into the scaffolds that could contribute to a microenvironment conducive to dormancy escape. These findings show the potential for this synthetic biomaterials-based model system to be used in the study of prostate cancer.

Acknowledgments

The authors would like to thank Shihua Sun, Kathryn Soriano, and Gerry Hammer for technical assistance. This work was supported by the Nanotechnology and Physical Science in Cancer Research Training Program NIH T32CA138312 (TJL and BDR), TMEN U54-CA126540 (SRP), P01 CA085859 (SRP), and the Veterans Affairs Research Service (SRP).

References

1. Siegel R, Naishadham D, Jemal A. Cancer Statistics, 2013. CA Cancer J Clin. 2013; 63:11–30. [PubMed: 23335087]
2. American Cancer Society. Detailed Guide: Prostate Cancer. 2012
3. Chung LWK, Baseman A, Assikis V, Zhau HE. Molecular insights into prostate cancer progression: the missing link of the tumor microenvironment. J Urol. 2005; 173:10–20. [PubMed: 15592017]
4. Bissell MJ, Radisky D. Putting tumors in context. Nat Rev Cancer. 2001; 1:46–54. [PubMed: 11900251]
5. Kleinman HK, Martin GR. Matrigel: basement membrane matrix with biological activity. Semin Cancer Biol. 2005; 15:378–386. [PubMed: 15975825]
6. Hughes CS, Postovit LM, Lajoie GA. Matrigel: a complex protein mixture required for optimal growth of cell culture. Proteomics. 2010; 10:1886–1890. [PubMed: 20162561]
7. Burdett E, Kasper K, Mikos AG, Ludwig JA. Engineering tumors: a tissue engineering perspective in cancer biology. Tissue Eng Part B. 2010; 16:351–359.
8. Hutmacher DW, Horch RE, Loessner D, Rizzi SC, Sieh S, Reichert JC, et al. Translating tissue engineering technology platforms into cancer research. J Cell Mol Med. 2009; 13:1417–1427. [PubMed: 19627398]
9. Hutmacher DW. Biomaterials offer cancer research the third dimension. Nat Mater. 2010; 9:90–93. [PubMed: 20094076]
10. Ghajar CM, Bissell MJ. Tumor engineering: the other face of tissue engineering. Tissue Eng Part A. 2010; 16:2153–2156. [PubMed: 20214448]
11. Debnath J, Brugge JS. Modeling glandular epithelial cancers in three-dimensional cultures. Nat Rev Cancer. 2005; 5:675–688. [PubMed: 16148884]
12. Abbott A. Biology's new dimension. Nature. 2003; 424:870–872. [PubMed: 12931155]
13. Kim JB. Three-dimensional tissue culture models in cancer biology. Semin Cancer Biol. 2005; 15:365–377. [PubMed: 15975824]
14. Hutmacher DW, Loessner D, Rizzi S, Kaplan DL, Mooney DJ, Clements JA. Can tissue engineering concepts advance tumor biology research? Trends Biotechnol. 2010; 28:125–133. [PubMed: 20056286]
15. Fischbach C, Chen R, Matsumoto T, Schmelzle T, Brugge JS, Polverini PJ, et al. Engineering tumors with 3D scaffolds. Nat Methods. 2007; 4:855–860. [PubMed: 17767164]
16. Sahoo SK, Panda AP, Labhasetwar V. Characterization of porous PLGA/PLA microparticles as a scaffold for three dimensional growth of breast cancer cells. Biomacromolecules. 2005; 6:1132–1139. [PubMed: 15762686]
17. Horning JL, Sahoo SK, Vijayaraghavalu S, Dimitrijevic S, Vasir JK, Jain TK, et al. 3-D tumor model for in vitro evaluation of anticancer drugs. Mol Pharm. 2008; 5:849–862. [PubMed: 18680382]

18. Weiss MS, Bernabe BP, Shikanov A, Bluver DA, Mui MD, Shin S, et al. The impact of adhesion peptides within hydrogels on the phenotype and signaling of normal and cancerous mammary epithelial cells. Biomaterials. 2012; 33:3548–3559. [PubMed: 22341213]
19. Loessner D, Stok KS, Lutolf MP, Hutmacher DW, Clements JA, Rizzi SC. Bioengineered 3D platform to explore cell-ECM interactions and drug resistance of epithelial ovarian cancer cells. Biomaterials. 2010; 31:8494–8506. [PubMed: 20709389]
20. Sieh S, Taubenberger AV, Rizzi SC, Sadowski M, Lehman ML, Rockstroh A, et al. Phenotypic characterization of prostate cancer LNCaP cells cultured within a bioengineered microenvironment. PLOS One. 2012; 7:e40217. [PubMed: 22957009]
21. Lee J, Li M, Milwid J, Dunham J, Vinegoni C, Gorbatov R, et al. Implantable microenvironments to attract hematopoietic stem/cancer cells. Proc Natl Acad Sci USA. 2012; 109:19638–19643. [PubMed: 23150542]
22. Boxberger HJ, Meyer TF. A new method for the 3-D in vitro growth of human RT112 bladder carcinoma cells using the alginate culture technique. Biol Cell. 1994; 82:109–119. [PubMed: 7606208]
23. Zhang X, Wang W, Yu W, Xie Y, Zhang X, Zhang Y, et al. Development of an in vitro multicellular tumor spheroid model using microencapsulation and its application in anticancer drug screening and testing. Biotechnol Prog. 2005; 21:1289–1296. [PubMed: 16080713]
24. Kievit FM, Florczyk SJ, Leung M, Veiseh O, Park JO, Disis ML, et al. Chitosan-alginate 3D scaffolds as a mimic of the glioma tumor microenvironment. Biomaterials. 2010; 31:5903–5910. [PubMed: 20417555]
25. Leung M, Kievit FM, Florczyk SJ, Veiseh O, Wu J, Park JO, et al. Chitosan-alginate scaffold culture system for hepatocellular carcinoma increases malignancy and drug resistance. Pharm Res. 2010; 27:1939–1948. [PubMed: 20585843]
26. Dhiman HK, Ray AR, Panda AK. Characterization and evaluation of chitosan matrix for in vitro growth of MCF-7 breast cancer cell lines. Biomaterials. 2004; 25:5147–5154. [PubMed: 15109838]
27. Tan PHS, Aung KZ, Toh SL, Hog JCH, Nathan SS. Three-dimensional porous silk tumor constructs in the approximation of in vivo osteosarcoma physiology. Biomaterials. 2011; 32:6131–6137. [PubMed: 21621837]
28. Liu Y, Shu XZ, Prestwich GD. Tumor engineering: orthotopic cancer models in mice using cell-loaded, injectable, cross-linked hyaluronan-derived hydrogels. Tissue Engineering. 2007; 13:1091–1101. [PubMed: 17582839]
29. Gurski LA, Jha AK, Zhang C, Jia X, Farach-Carson MC. Hyaluronic acid-based hydrogels as 3D matrices for in vitro evaluation of chemotherapeutic drugs using poorly adherent prostate cancer cells. Biomaterials. 2009; 30:6076–6085. [PubMed: 19695694]
30. Dhiman HK, Ray AR, Panda AK. Three-dimensional chitosan scaffold-based MCF-7 cell culture for the determination of the cytotoxicity of tamoxifen. Biomaterials. 2005; 26:979–986. [PubMed: 15369686]
31. Szot CS, Buchanan CF, Freeman JW, Rylander MN. 3D in vitro bioengineered tumors based on collagen I hydrogels. Biomaterials. 2011; 32:7905–7912. [PubMed: 21782234]
32. Marshall AJ, Irvin CA, Barker T, Sage EH, Hauch KD, Ratner BD. Biomaterials with tightly controlled pore size that promote vascular in-growth. ACS Polymer Preprints. 2004; 45:100–101.
33. Madden LR, Mortisen DJ, Sussman EM, Dupras SK, Fugate JA, Cuy JL, et al. Proangiogenic scaffolds as functional templates for cardiac tissue engineering. Proc Natl Acad Sci USA. 2010; 107:15211–15216. [PubMed: 20696917]
34. Bae VL, Jackson-Cook CK, Maygarden SJ, Plymate SR, Chen J, Ware JL. Metastatic sublines of an SV40 large T antigen immortalized human prostate epithelial cell line. Prostate. 1998; 34:275–282. [PubMed: 9496902]
35. Thalmann GN, Anezinis PE, Chang SM, Zhau HE, Kim EE, Hopwood VL, et al. Androgen-independent cancer progression and bone metastasis in the LNCaP model of human prostate cancer. Cancer Res. 1994; 54:2577–2581. [PubMed: 8168083]

36. Thalmann GN, Sikes RA, Wu TT, Degeorges A, Chang SM, Ozen M, et al. LNCaP progression model of human prostate cancer: androgen-independence and osseous metastasis. Prostate. 2000; 44:91–103. [PubMed: 10881018]
37. Swisshelm K, Ryan K, Tsuchiya K, Sager R. Enhanced expression of an insulin growth factor like-binding protein (mac25) in senescent human mammary epithelial cells and induced expression with retinoic acid. Proc Natl Acad Sci USA. 1995; 92:4472–4476. [PubMed: 7538673]
38. Burger AM, Zhang X, Li H, Ostrowski JL, Beatty B, Venanzoni M, et al. Down-regulation of T1A12/mac25, a novel insulin-like growth factor binding protein related gene, is associated with disease progression in breast carcinomas. Oncogene. 1998; 16:2459–2467. [PubMed: 9627112]
39. Komatsu S, Okazaki Y, Tateno M, Kawai J, Konno H, Kusakabe M, et al. Methylation and downregulated expression of mac25/insulin-like growth factor binding protein-7 is associated with liver tumorigenesis in SV40T/t antigen transgenic mice, screened by restriction landmark genomic scanning for methylation (RLGS-M). Biochem Biophys Res Commun. 2000; 267:109–117. [PubMed: 10623583]
40. Sato Y, Chen Z, Miyazaki K. Strong suppression of tumor growth by insulin-like growth factor-binding protein-related protein 1/tumor-derived cell adhesion factor/mac25. Cancer Sci. 2007; 98:1055–1063. [PubMed: 17465992]
41. Wajapeyee N, Serra R, Zhu X, Mahalingam M, Green MR. Oncogenic BRAF induces senescence and apoptosis through pathways mediated by the secreted protein IGFBP7. Cell. 2008; 132:363–374. [PubMed: 18267069]
42. Sprenger CC, Damon SE, Hwa V, Rosenfeld RG, Plymate SR. Insulin-like growth factor binding protein related protein 1 (IGFBP-rp1) is a potential tumor suppressor for prostate cancer. Cancer Res. 1999; 59:2370–2375. [PubMed: 10344746]
43. Hwa V, Tomosini-Sprenger C, Bermejo AL, Rosenfeld RG, Plymate SR. Characterization of insulin-like growth factor binding protein related protein-1 in prostate cells. J Clin Endocrinol Metab. 1998; 83:4355–4362. [PubMed: 9851777]
44. Sprenger CC, Vail ME, Evans K, Simurdak J, Plymate SR. Over-expression of insulin-like growth factor binding protein-related protein-1 (IGFBP-rP1/mac25) in the M12 prostate cancer cell line alters tumor growth by a delay in G1 and cyclin A associated apoptosis. Oncogene. 2002; 21:140–147. [PubMed: 11791184]
45. Sprenger CCT, Drivdahl RH, Woodke LB, Eyman D, Reed MJ, Carter WG, et al. Senescence-induced alterations of laminin chain expression modulate tumorigenicity of prostate cancer cells. Neoplasia. 2008; 10:1350–1361. [PubMed: 19048114]
46. Aguirre-Ghiso JA. Models, mechanisms and clinical evidence for cancer dormancy. Nat Rev Cancer. 2007; 7:834–846. [PubMed: 17957189]
47. Goss PE, Chambers AF. Does tumor dormancy offer a therapeutic target? Nat Rev Cancer. 2010; 10:871–877. [PubMed: 21048784]
48. Klein CA. Framework models of tumor dormancy from patient-derived observations. Curr Opin Genet Dev. 2011; 21:42–49. [PubMed: 21145726]
49. Wikman H, Vessella R, Pantel K. Cancer micrometastasis and tumour dormancy. APMIS. 2008; 116:754–770. [PubMed: 18834417]
50. Morgan TM, Lange PH, Porter MP, Lin DW, Ellis WJ, Gallaher IS, et al. Disseminated tumor cells in prostate cancer patients after radical prostatectomy and without evidence of disease predicts biochemical recurrence. Clin Cancer Res. 2009; 15:677–683. [PubMed: 19147774]
51. Long TJ, Takeno M, Sprenger C, Plymate SR, Ratner BD. Capillary force seeding of sphere-templated hydrogels for tissue engineered prostate cancer xenografts. Tissue Eng Part C. 2013; 19:738–744.
52. Coffelt SB, Hughes R, Lewis CE. Tumor-associated macrophages: effectors of angiogenesis and tumor progression. Biochim Biophys Acta. 2009; 1796:11–18. [PubMed: 19269310]
53. Mantovani A, Schioppa T, Porta C, Allavena P, Sica A. Role of tumor-associated macrophages in tumor progression and invasion. Cancer Metastasis Rev. 2006; 25:315–322. [PubMed: 16967326]
54. Suresh S. Biomechanics and biophysics of cancer cells. Acta Biomater. 2007; 3:413–438. [PubMed: 17540628]

55. Kumar S, Weaver VM. Mechanics, malignancy, and metastasis: the force journey of a tumor cell. Cancer Metastasis Rev. 2009; 28:113–127. [PubMed: 19153673]

56. Levental KR, Yu H, Kass L, Lakins JN, Egeblad M, Erler JT, et al. Matrix crosslinking forces tumor progression by enhanced integrin signaling. Cell. 2009; 139:891–906. [PubMed: 19931152]

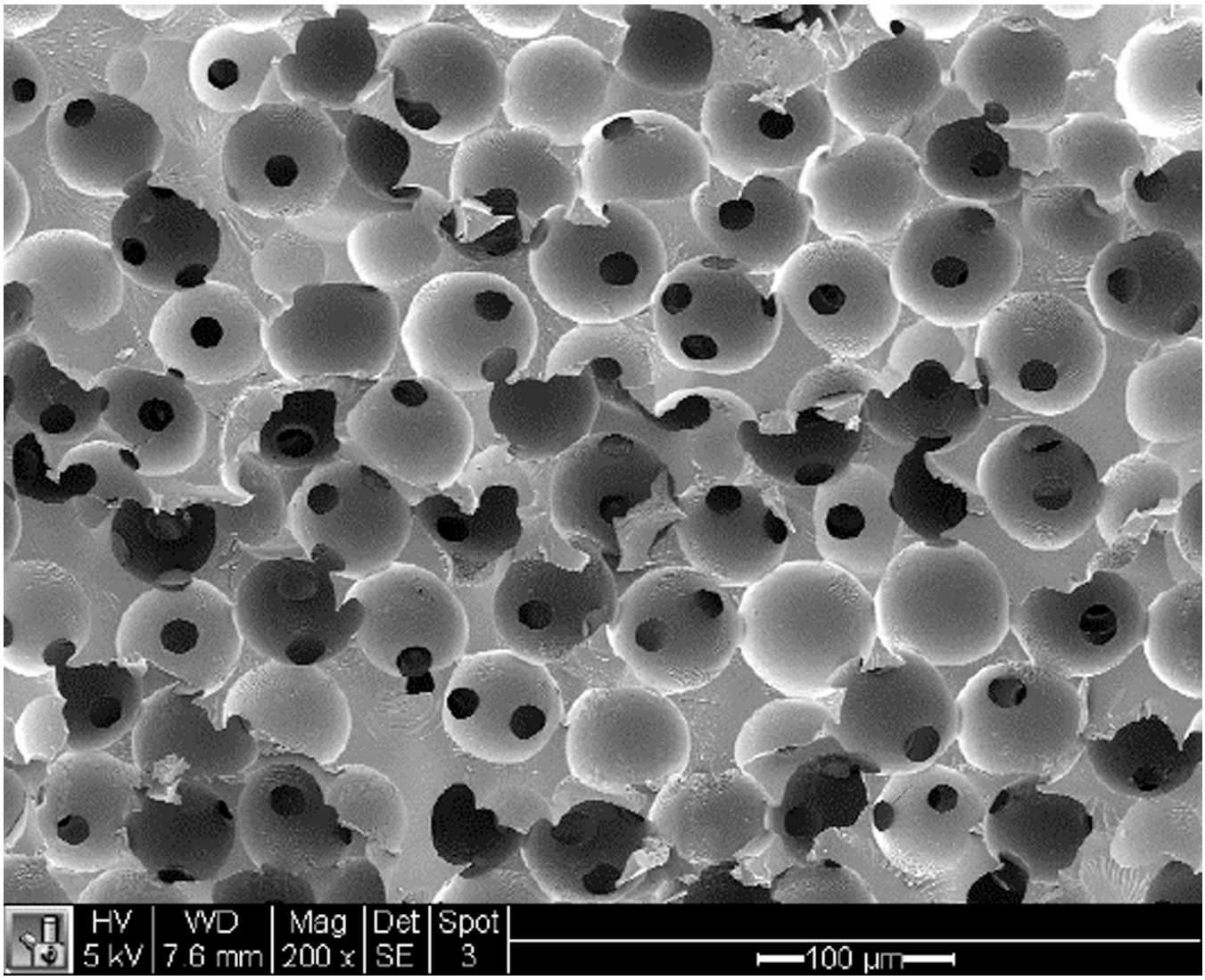

Figure 1.
SEM image of an unseeded sphere-templated pHEMA scaffold (scale bar = 100 µm)

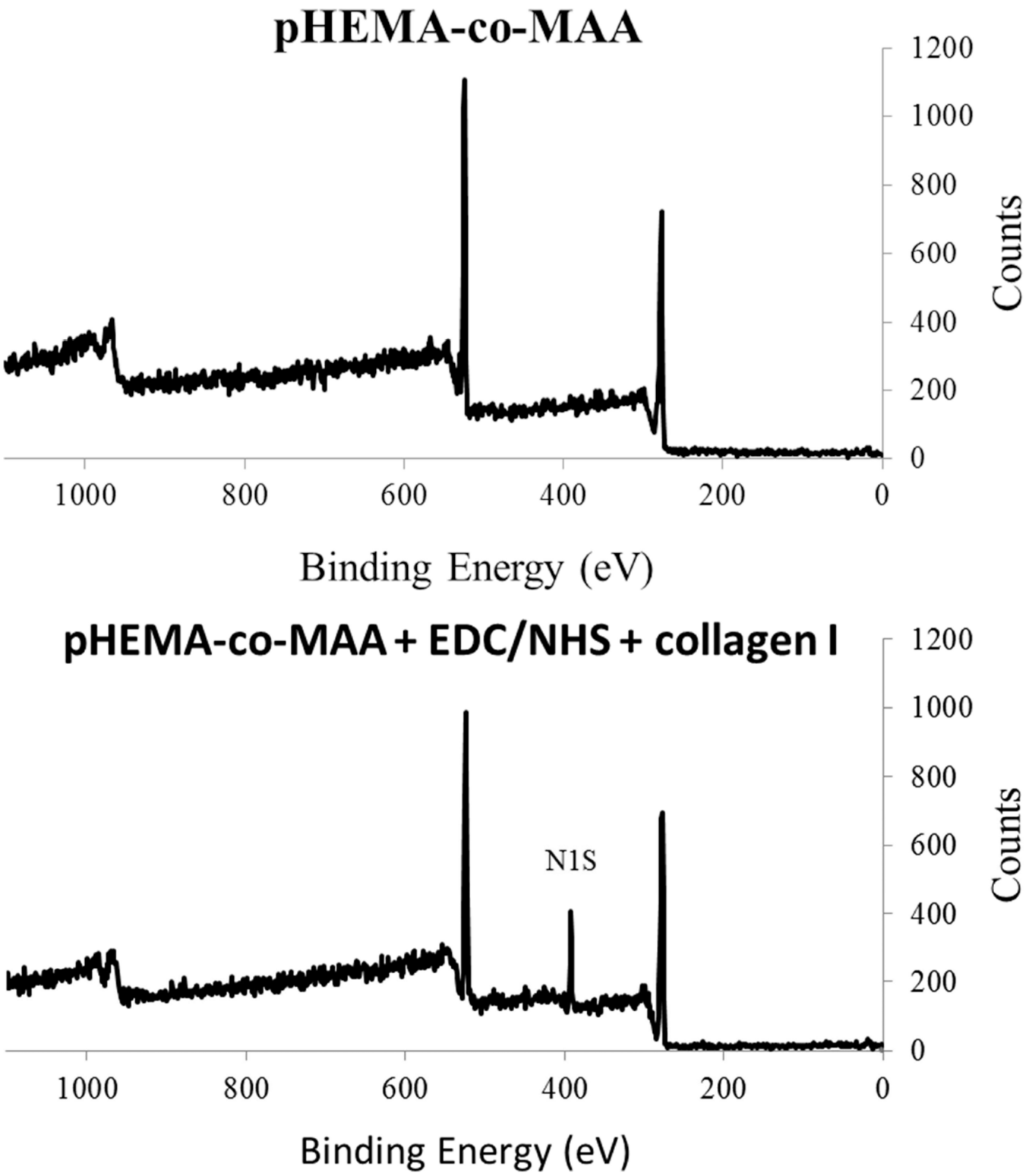

Figure 2.

XPS survey spectra showing (A) pHEMA-co-MAA controls with only peaks corresponding to carbon (285 eV) and oxygen (530 eV), and (B) pHEMA-co-MAA + EDC/NHS + collagen I showing an additional nitrogen peak (400 eV) showing protein attachment.

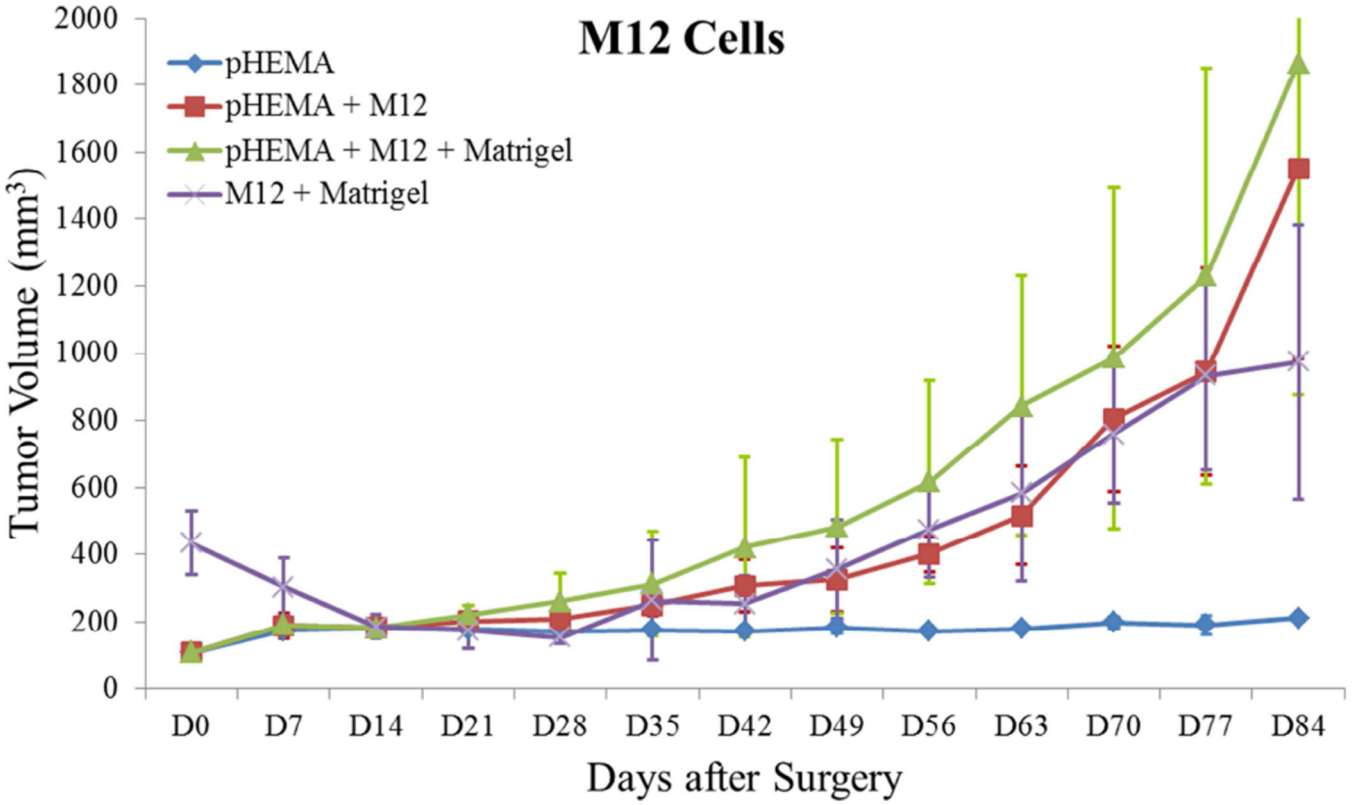

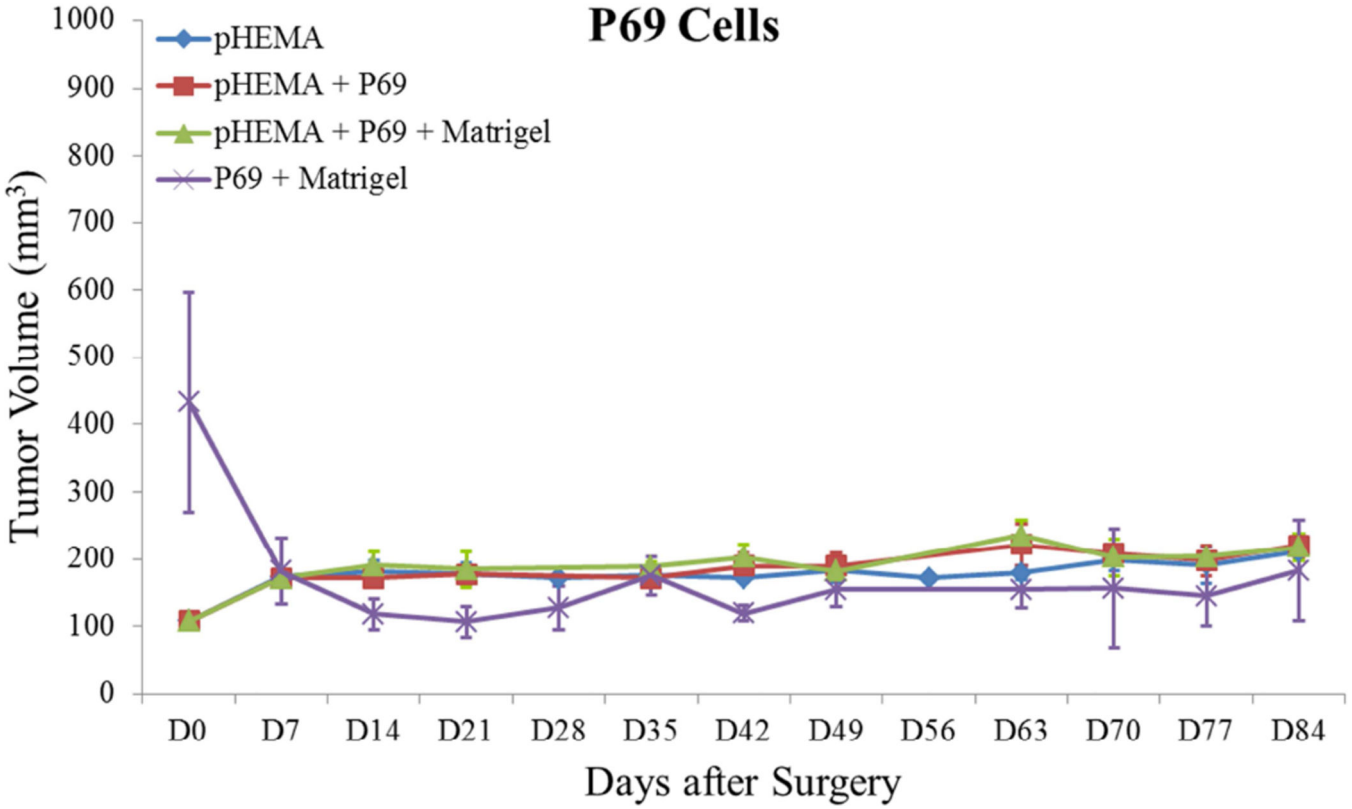

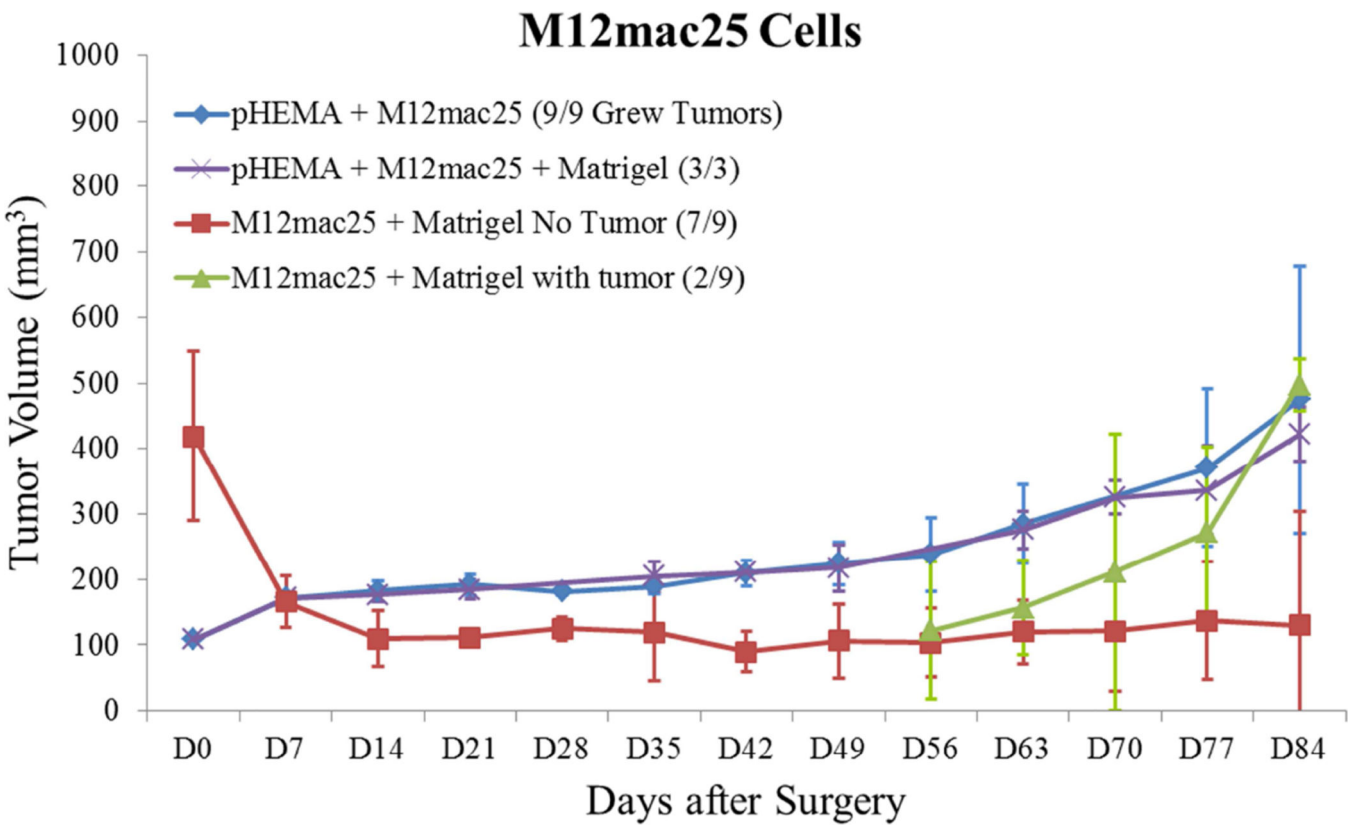

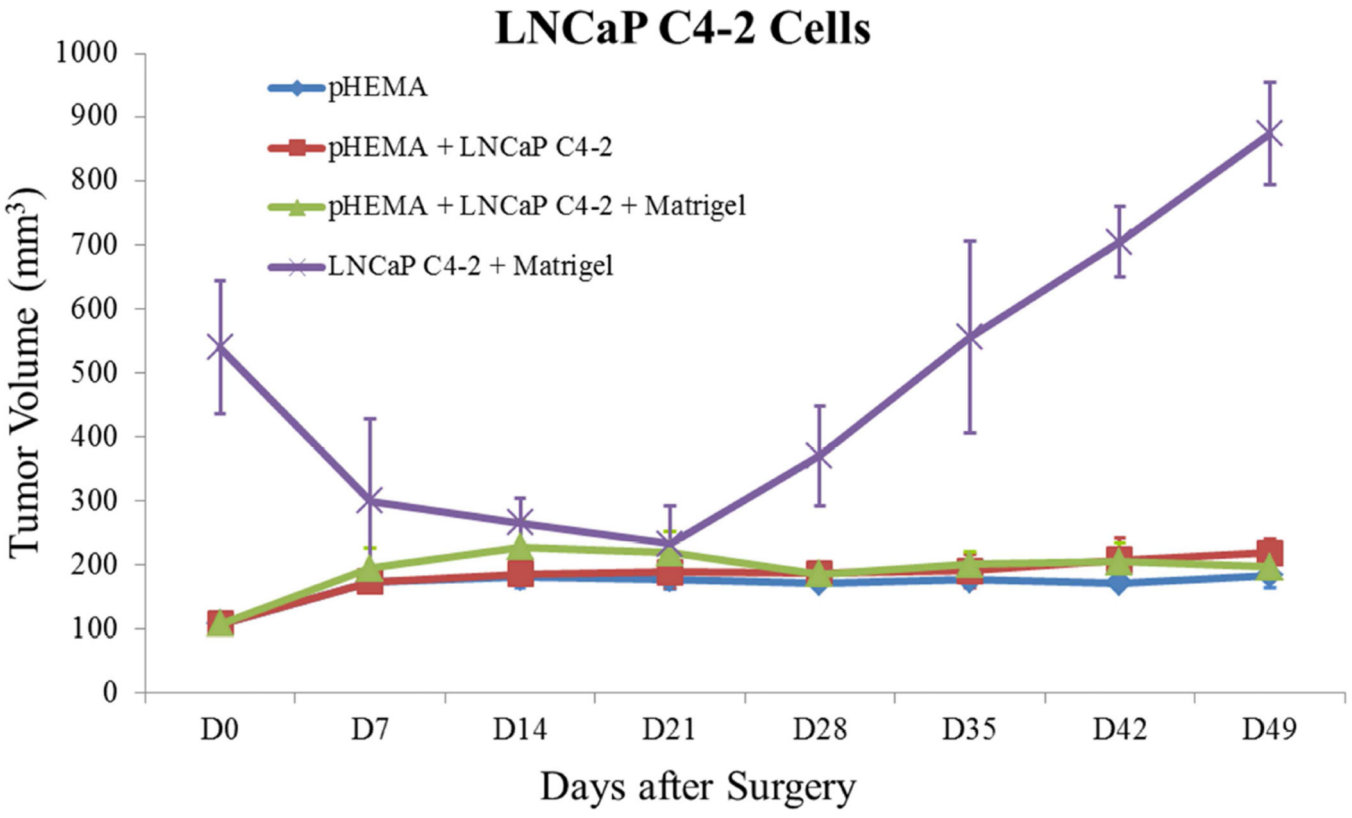

Figure 3.

Tumor growth curves for (A) M12 cells, (B) P69 cells, (C) M12mac25 cells, and (D) LNCaP C4-2 cells. Tumor volume was calculated using the equation $V = (L \times W^2)/2$. M12 cells demonstrate equivalent growth kinetics between pHEMA, Matrigel, and pHEMA + Matrigel groups over twelve weeks. P69 cells served as a non-tumorigenic cell control, failing to form tumors in any experimental group. Data compiled from pilot and follow-up *in vivo* studies show that M12mac25 cells consistently form tumors when implanted within pHEMA scaffolds with or without Matrigel, but in most cases remain dormant and fail to form tumors when injected with Matrigel. LNCaP C4-2 cells grew large tumors when injected with Matrigel, but failed to form tumors when implanted in pHEMA with or without Matrigel over seven weeks.

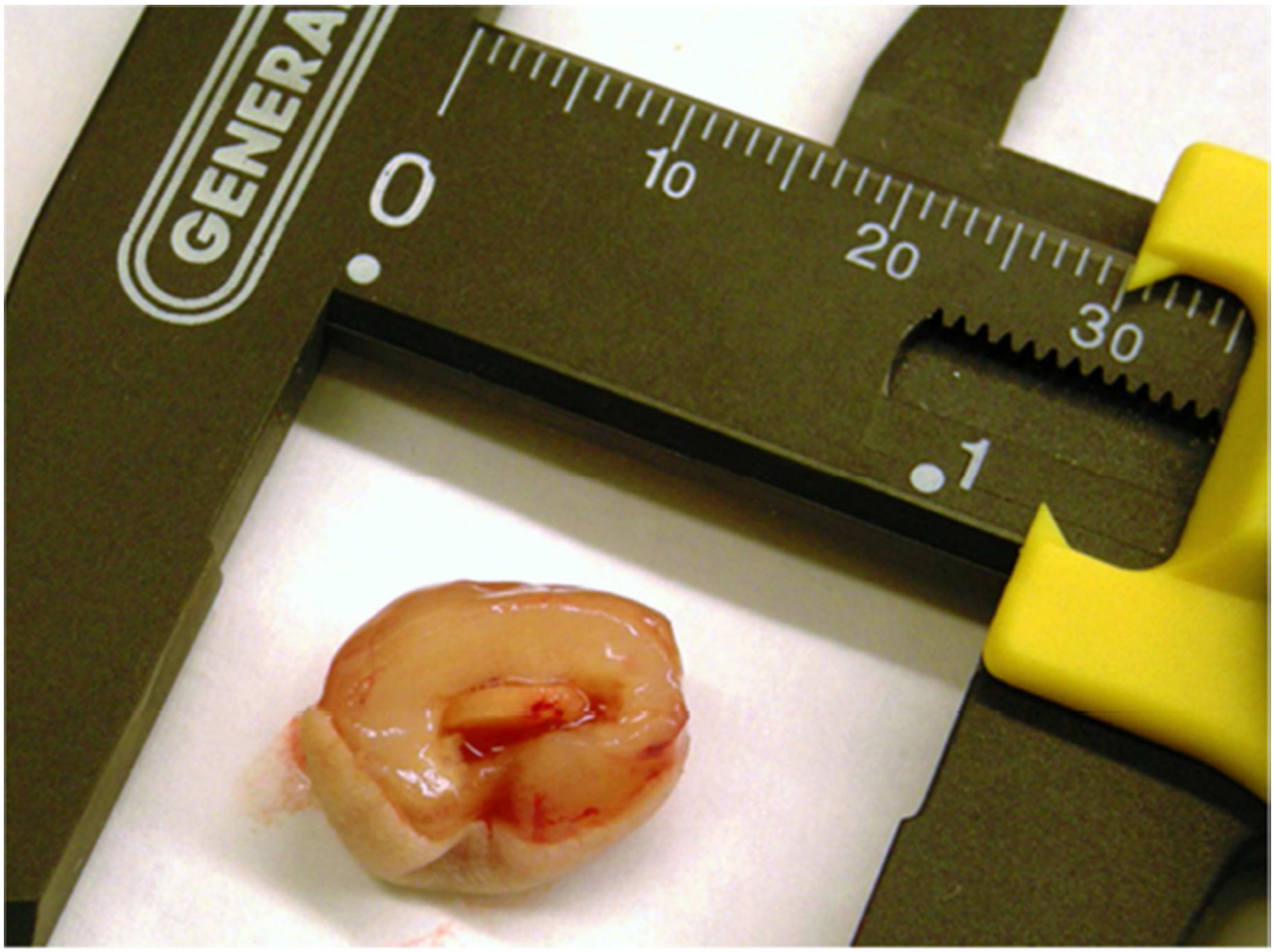

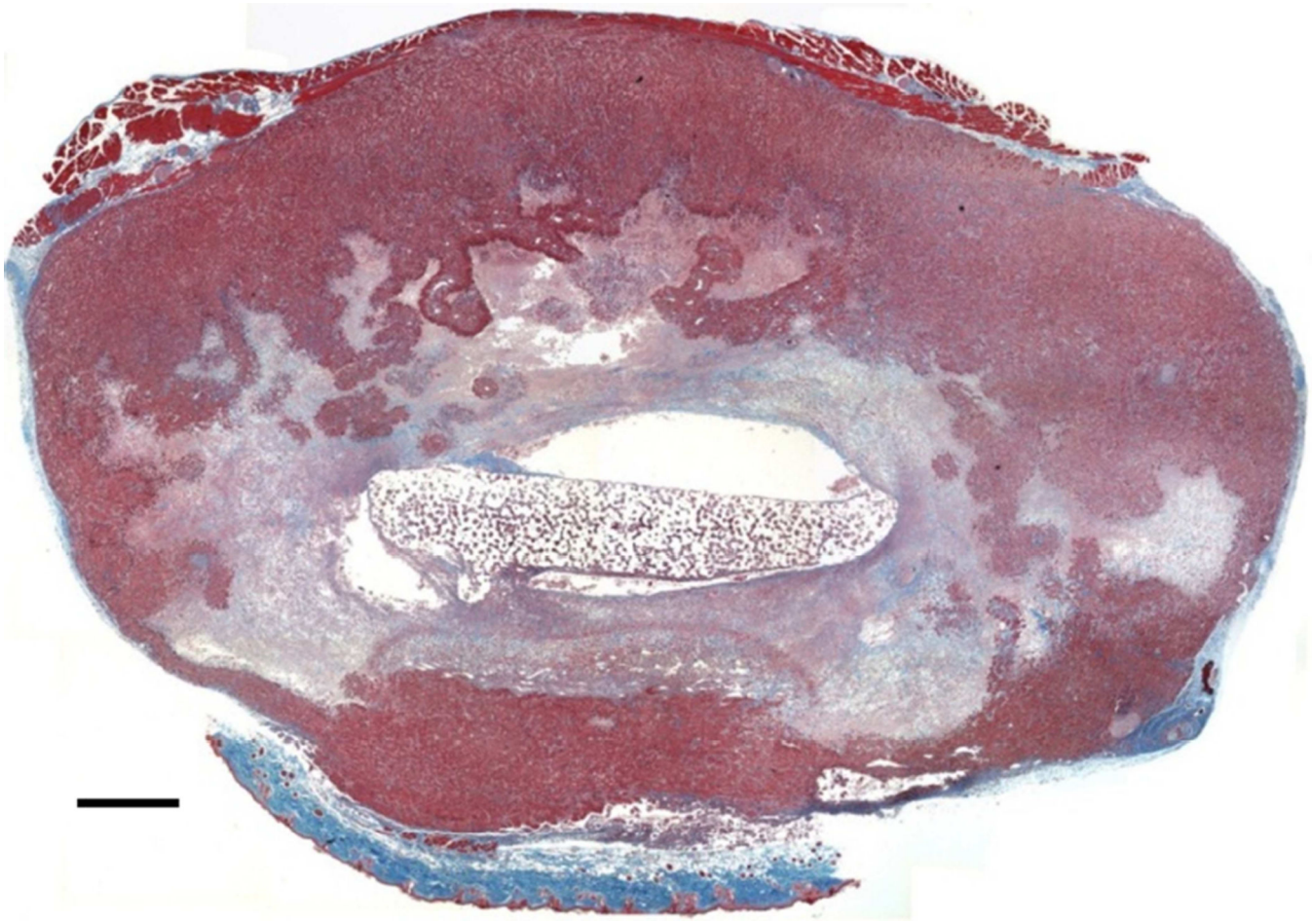

Figure 4.

(A) Photograph of explanted pHEMA-derived M12 cell xenograft at twelve weeks with calipers (mm scale). Tumors grew around the implanted pHEMA scaffolds. (B) Masson's trichrome stain of pHEMA-derived M12 cell xenograft at 12 weeks (scale bar = 1 mm) showing the scaffold in a necrotic core surrounded by viable tumor tissue.

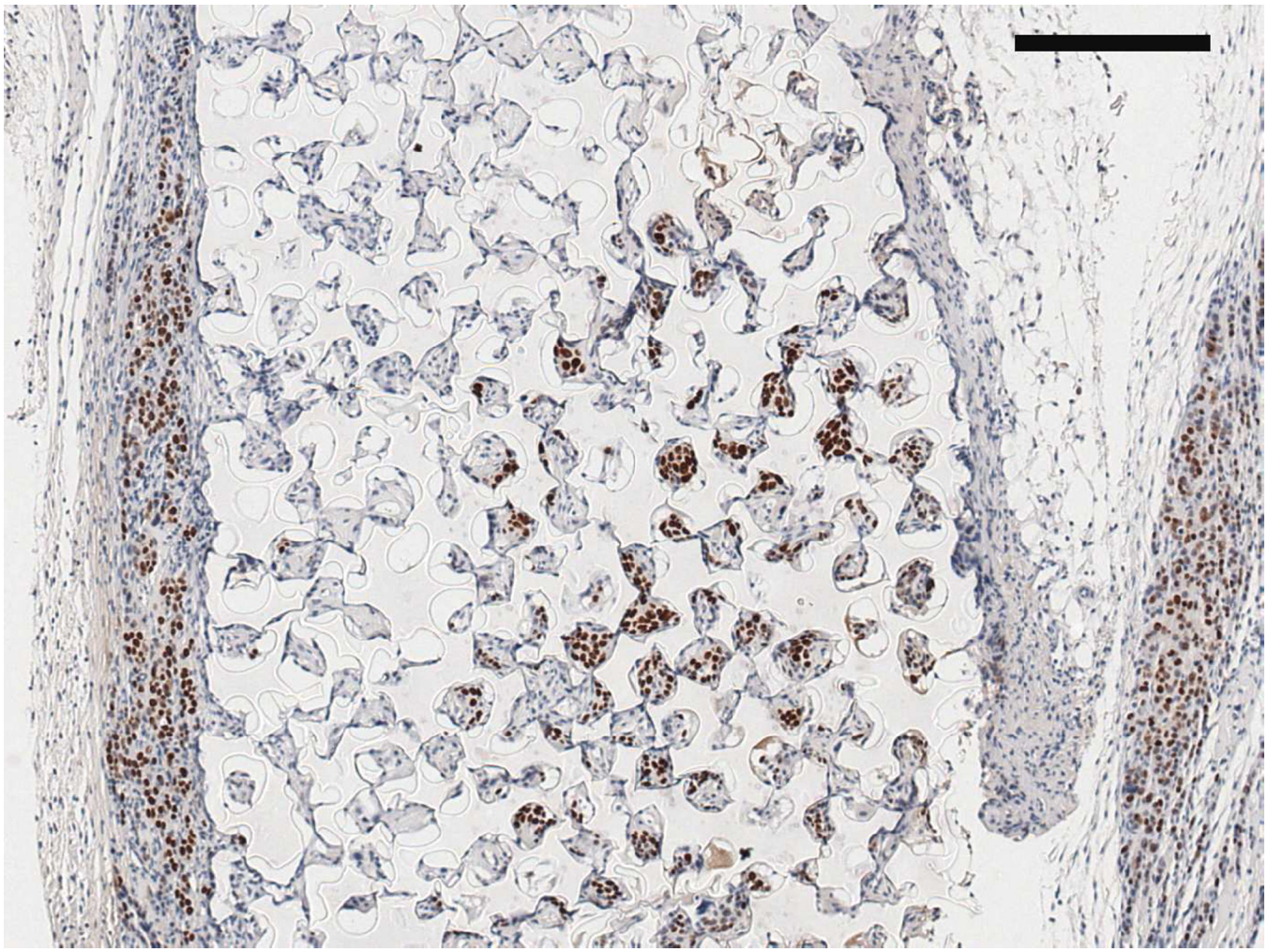

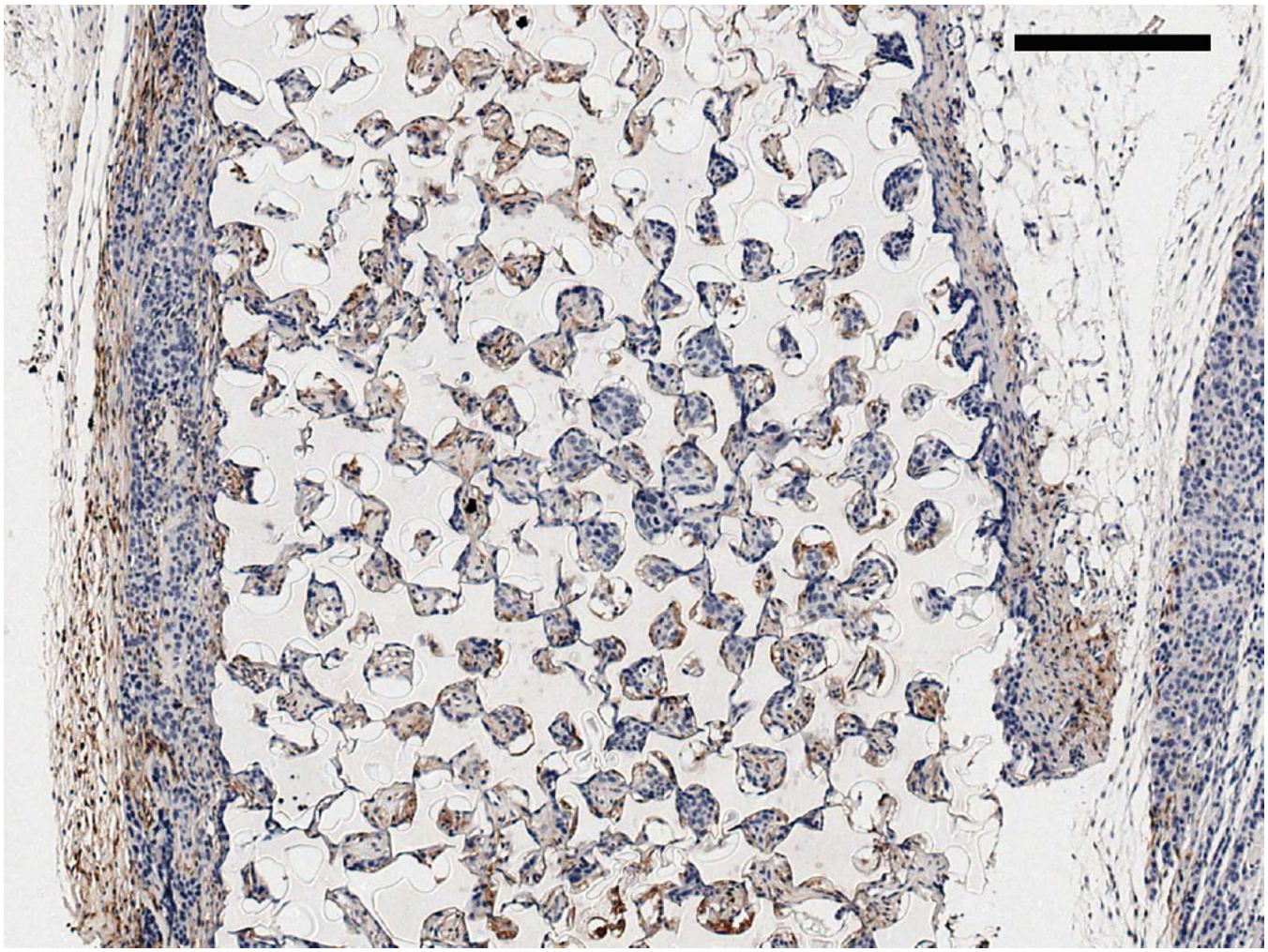

Figure 5.

Serial sections of a three week M12-seeded pHEMA explant. (A) SV40T IHC stain showing brown M12 cells remaining in the scaffold and beginning to migrate into surrounding tissue. (B) F4/80 IHC stain showing significant brown mouse macrophage infiltration into the scaffold and presence around the scaffold as part of the foreign body response. Note that areas in the scaffold that are significantly staining with SV40T are complementary to areas significantly staining with F4/80, showing that macrophages entering the scaffold are infiltrating around seeded cancer cells (scale bars = 250 μm).

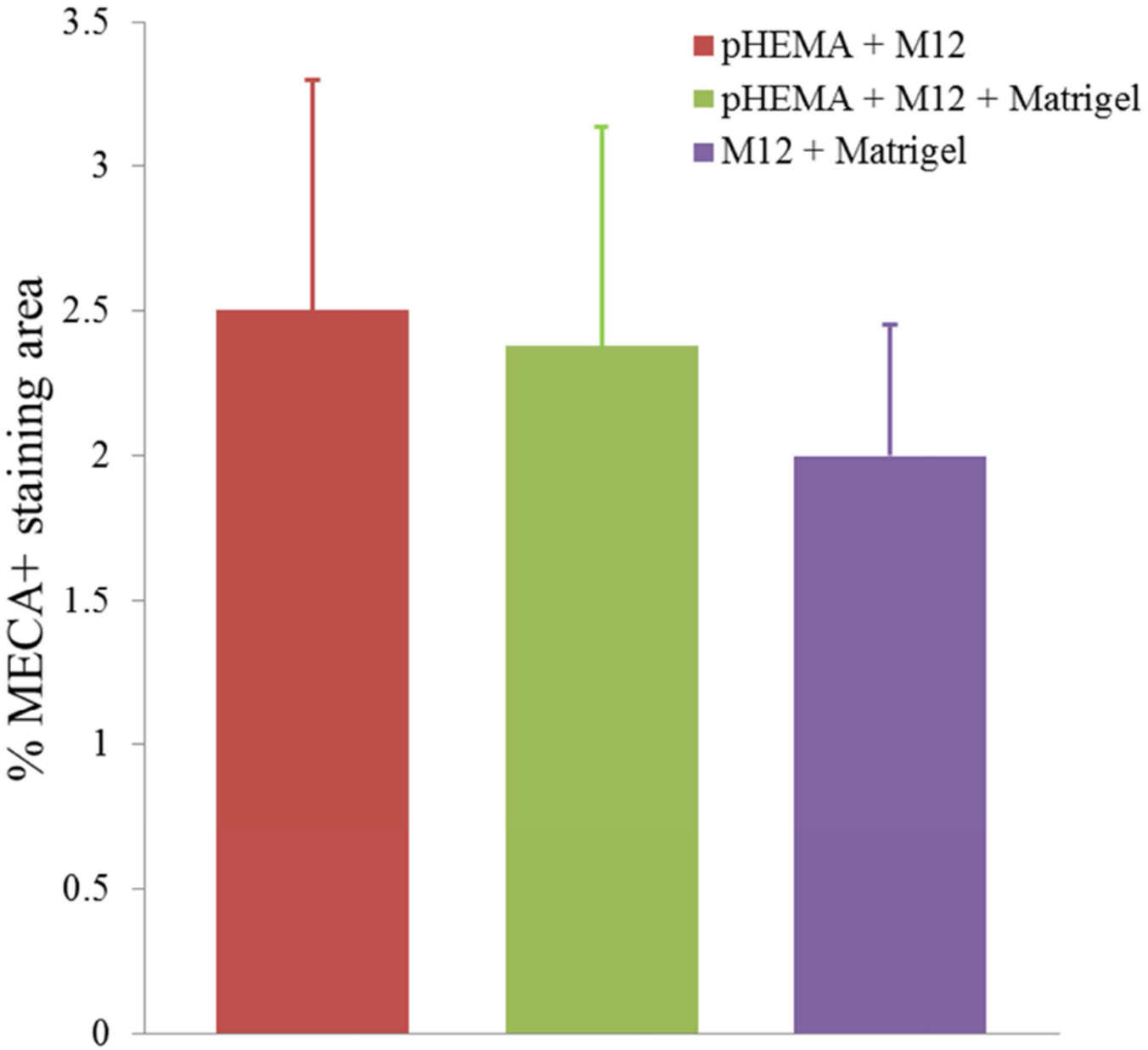

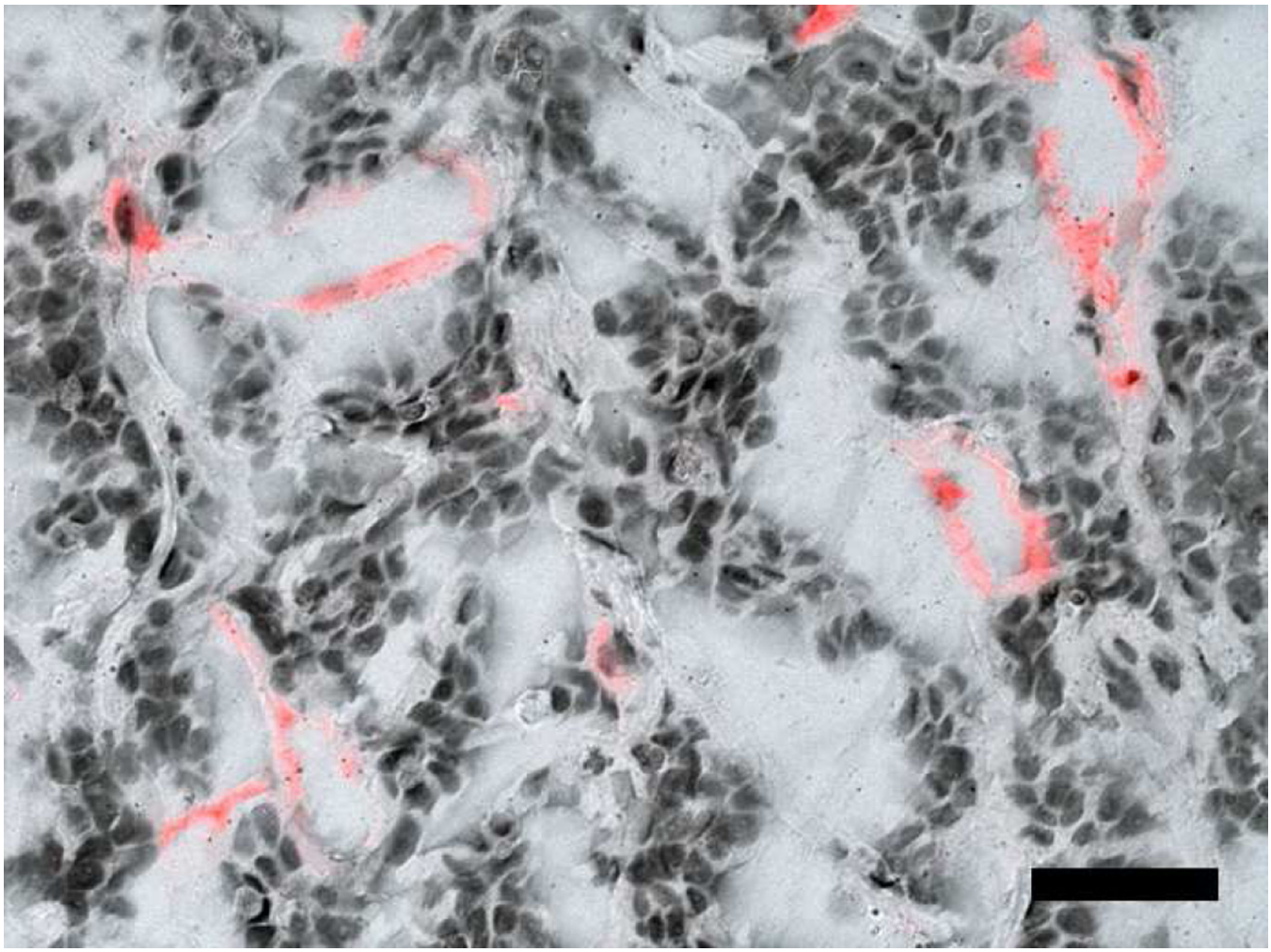

Figure 6.

(A) % MECA+ staining area for D84 M12 xenograft explants showed no significant differences in vascularity between the pHEMA-derived tumors and standard subcutaneous Matrigel xenografts. (B) Representative MECAstained fluorescent IHC image showing M12 tumor endothelial cells and vessels in red (scale bar = 20 μm).

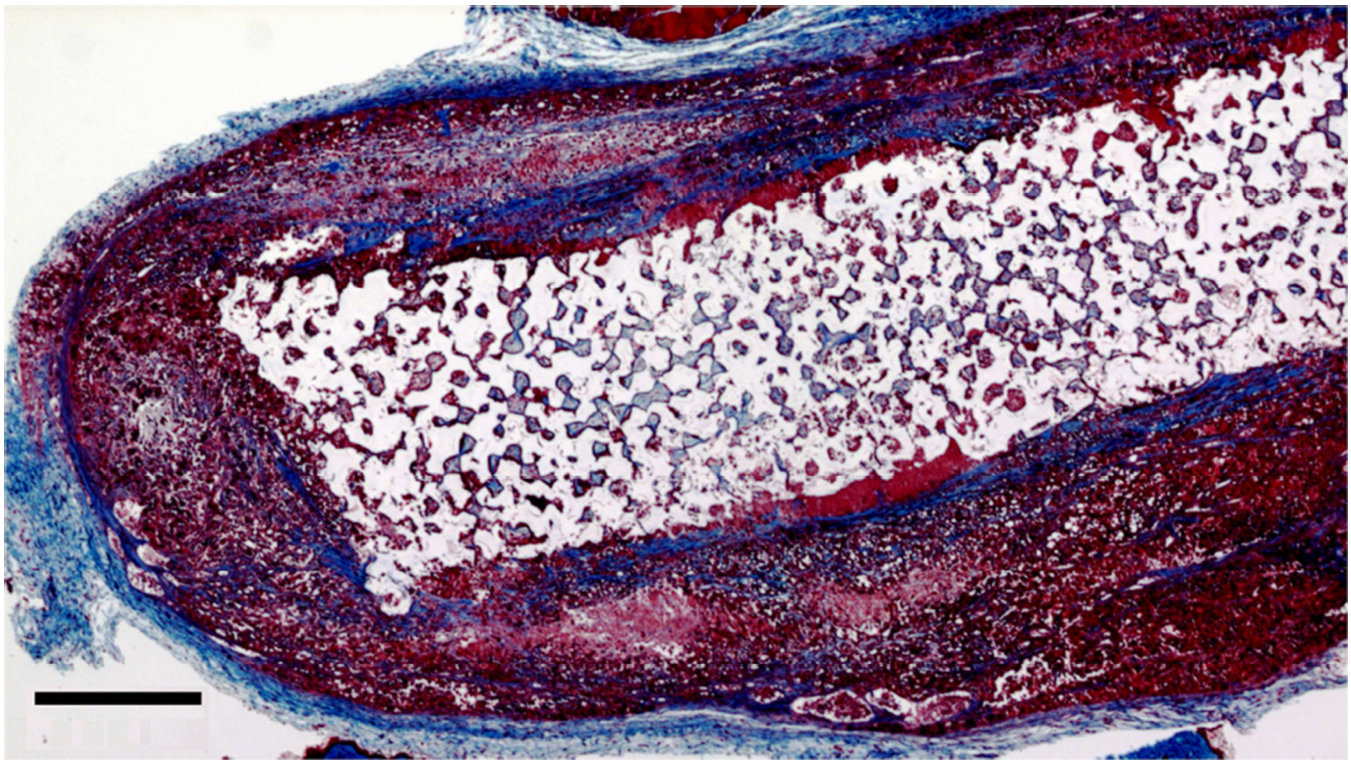

Figure 7.
Masson's trichrome stain of a twelve week M12mac25-derived xenograft (scale bar 500 μm).

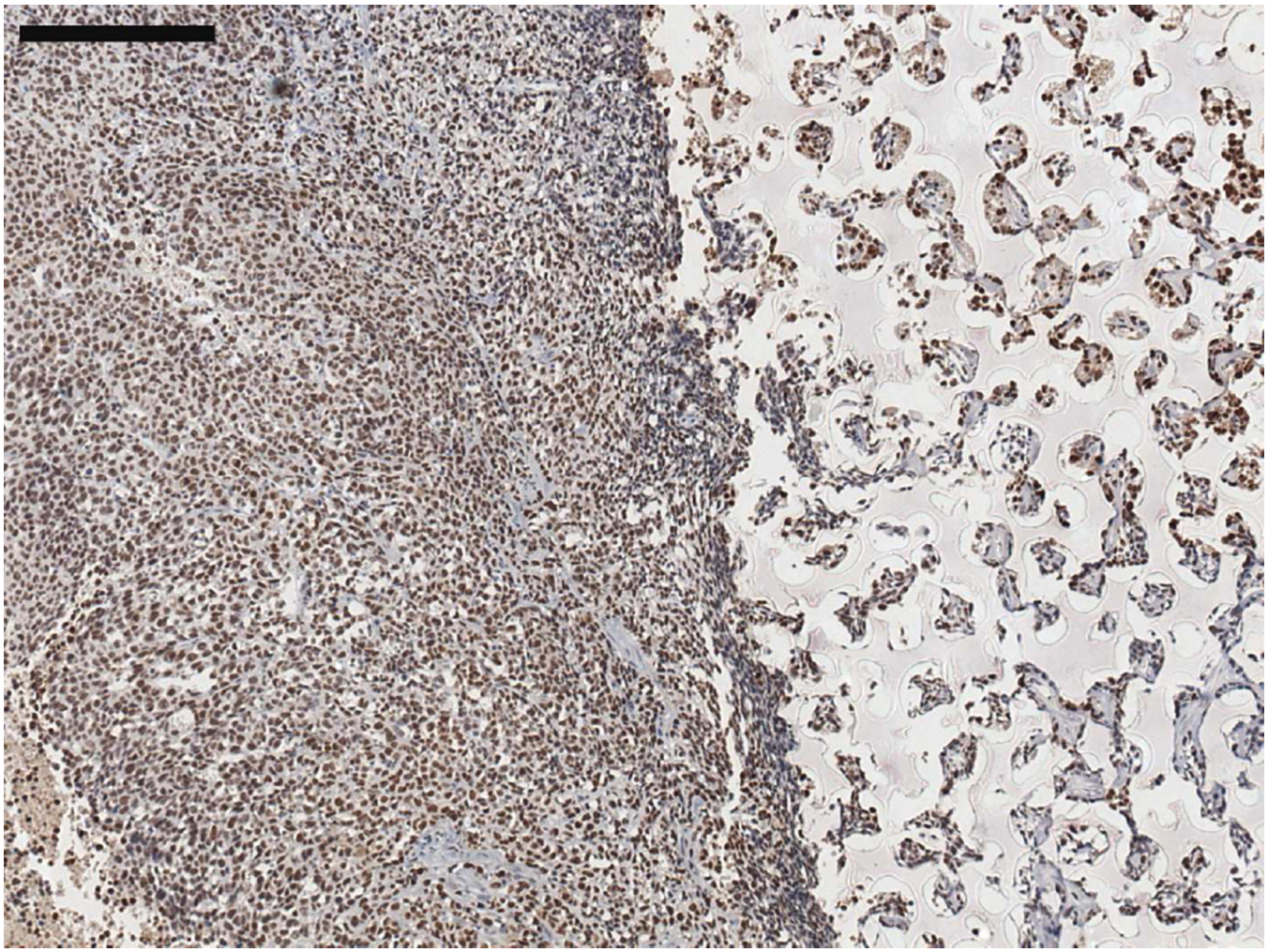

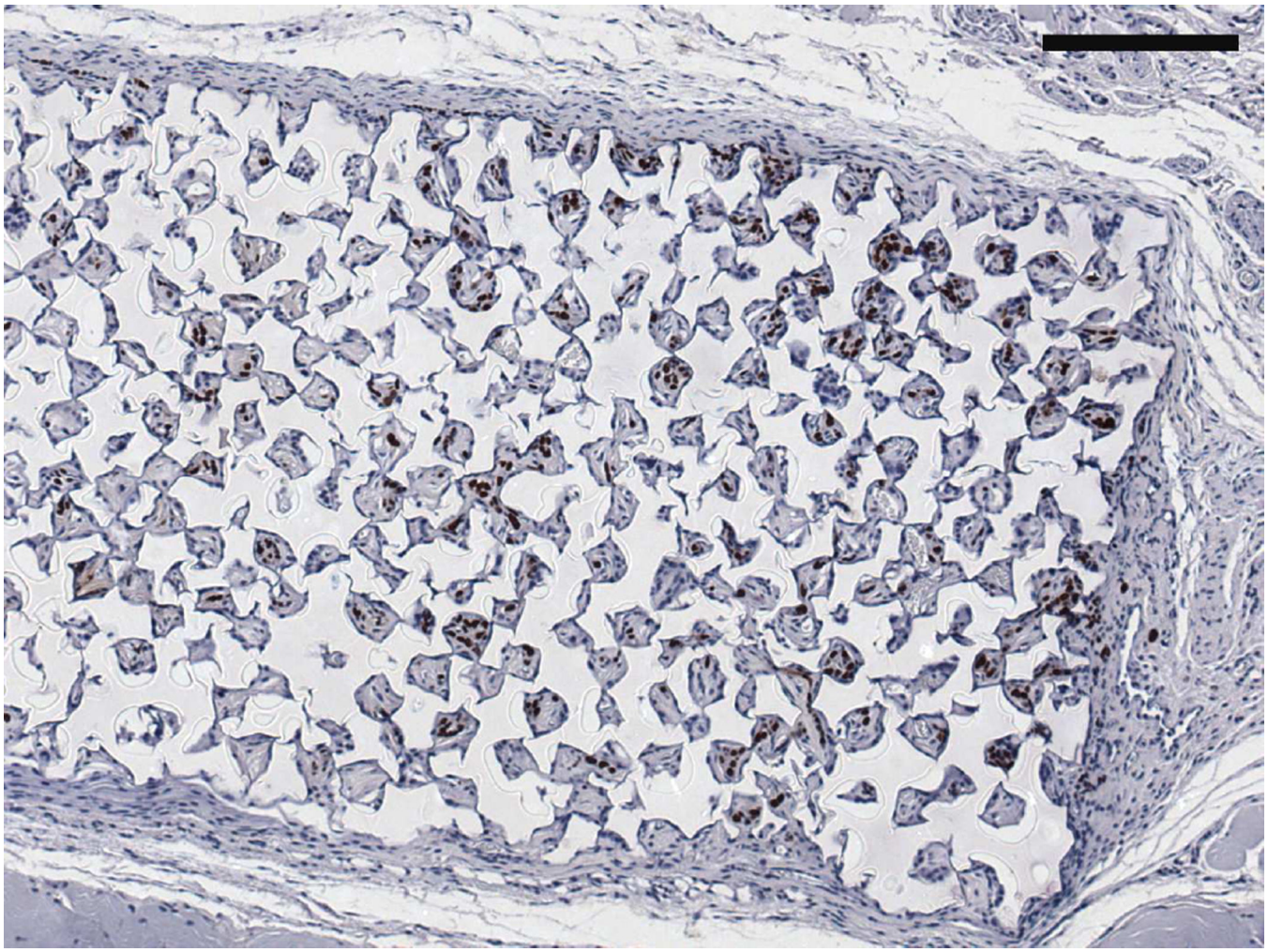

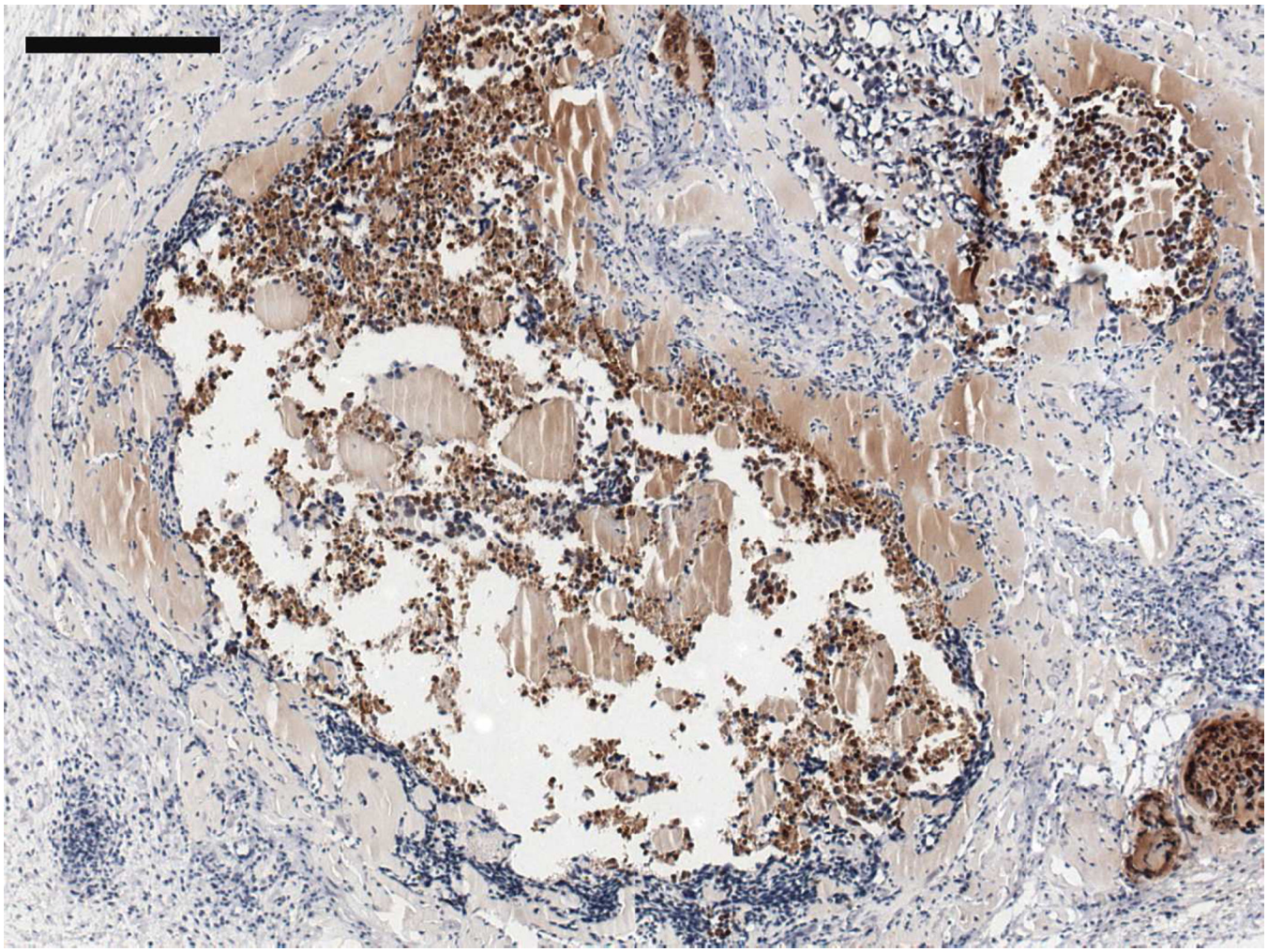

Figure 8.

SV40T IHC on (A) twelve week M12mac25 pHEMA explant showing the tumor/scaffold interface (B) three week M12mac25 pHEMA explant showing human cells in the scaffold without significant proliferation or tumor formation (C) twelve week M12mac25 Matrigel explant showing cells remaining dormant and confined to a small area (scale bars = 250 μm).

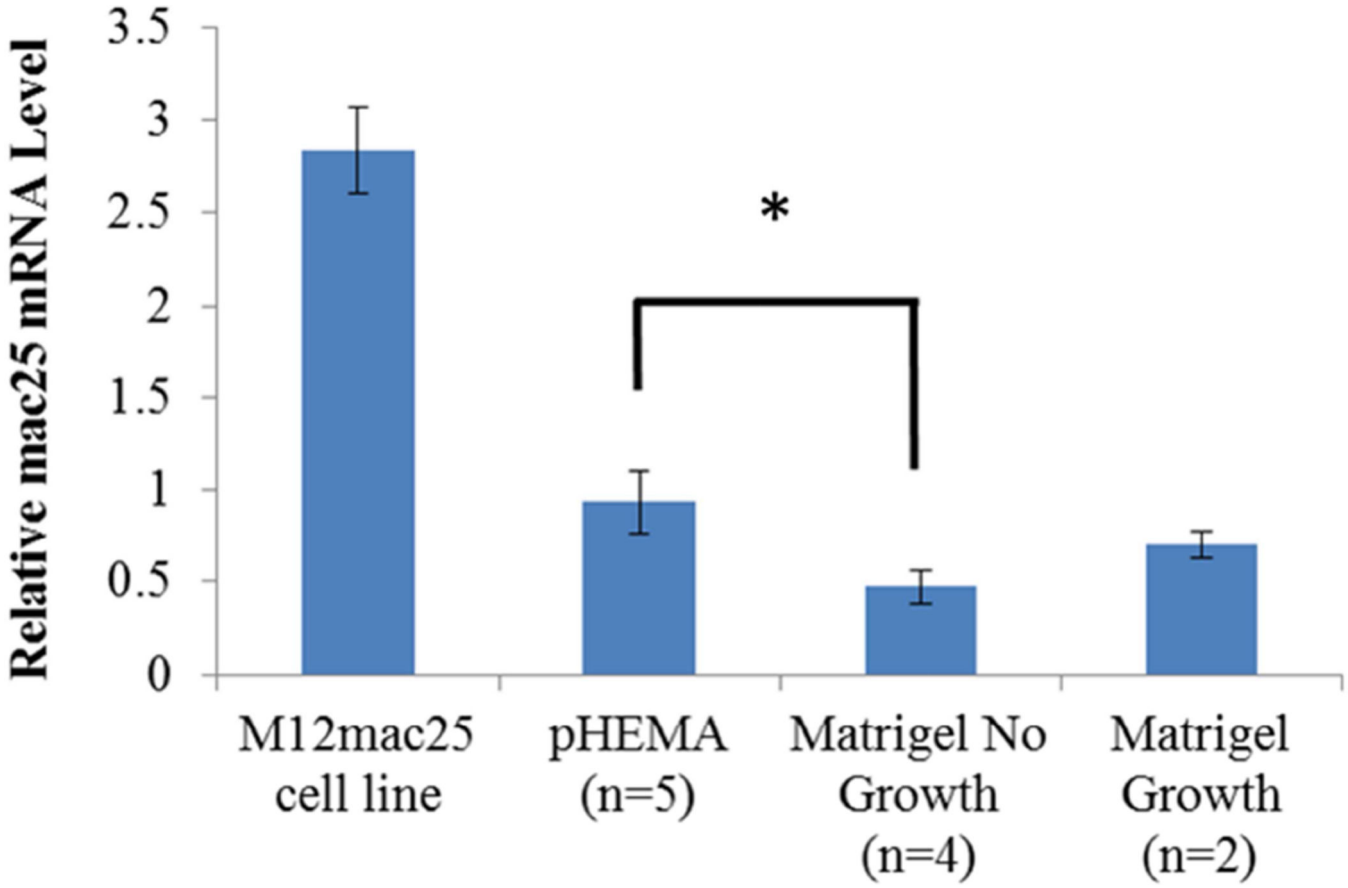

Figure 9.

mac25 qRT-PCR results showing relative mRNA levels in each M12mac25 pHEMA and Matrigel explant from the follow-up *in vivo* study and the M12mac25 cell line. IGFBP7 mRNA was several fold lower in all D84 *in vivo* explants relative to the *in vitro* cell line, but remained significantly higher in the pHEMA explant group relative to the Matrigel no growth (* $p < 0.01$) group.

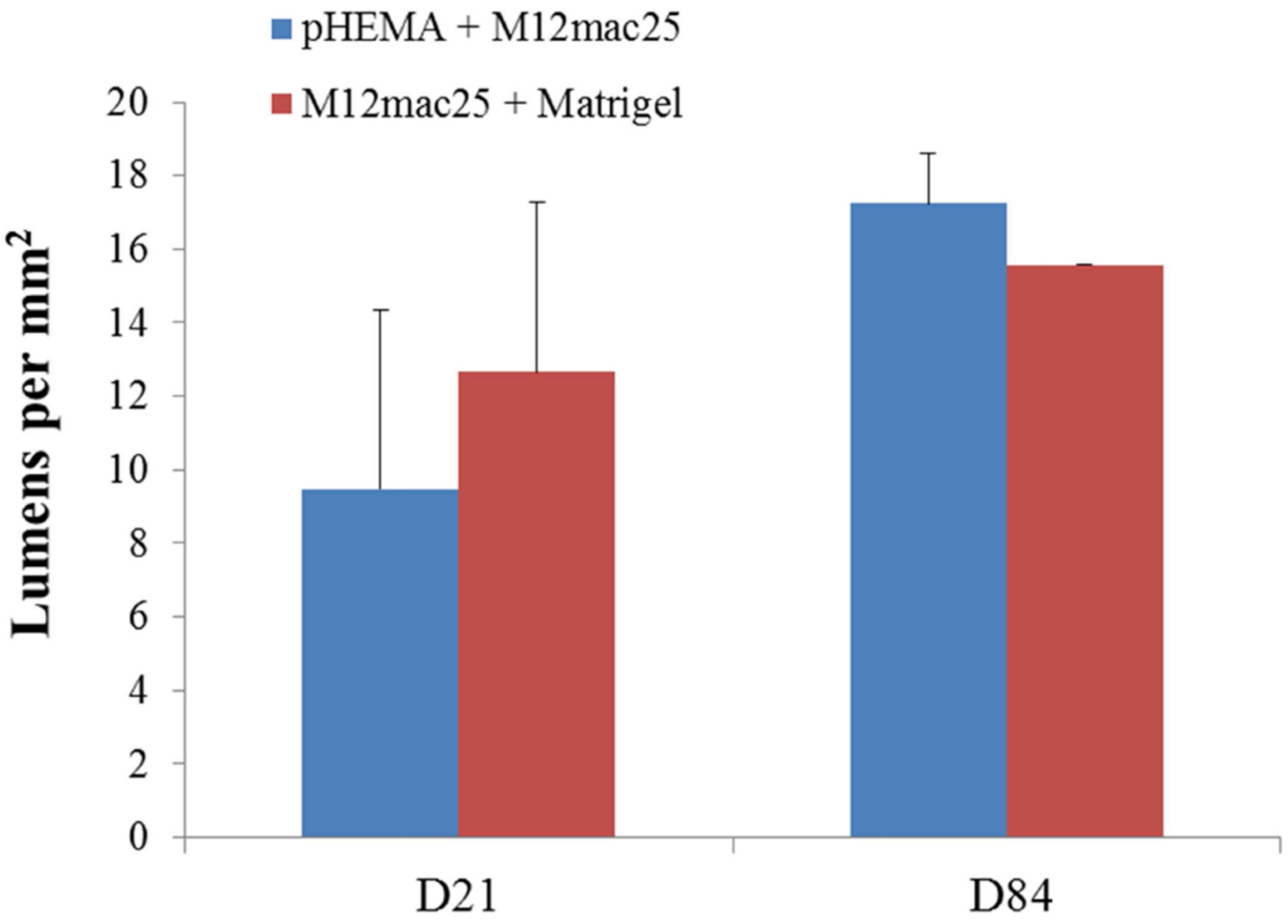

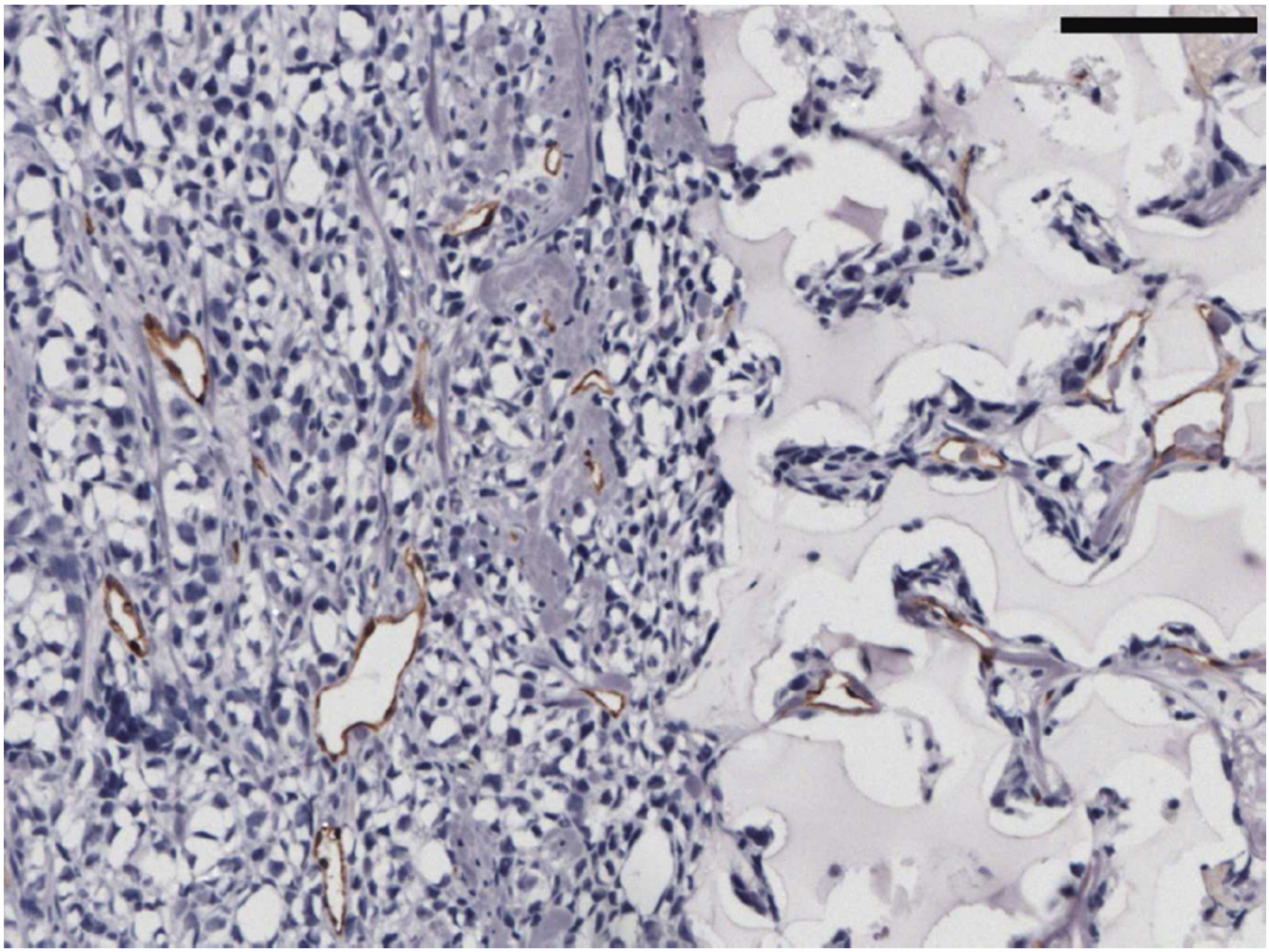

Figure 10.

(A) MECA+ lumen density in twelve week M12mac25 explants showed no significant differences in vascularity between the pHEMA and Matrigel groups at D21 or D84 after implantation. (B) Representative MECAstained IHC image showing brown endothelial vessels in the pHEMA explant and in the surrounding M12mac25 tumor (scale bar = 100 μm).

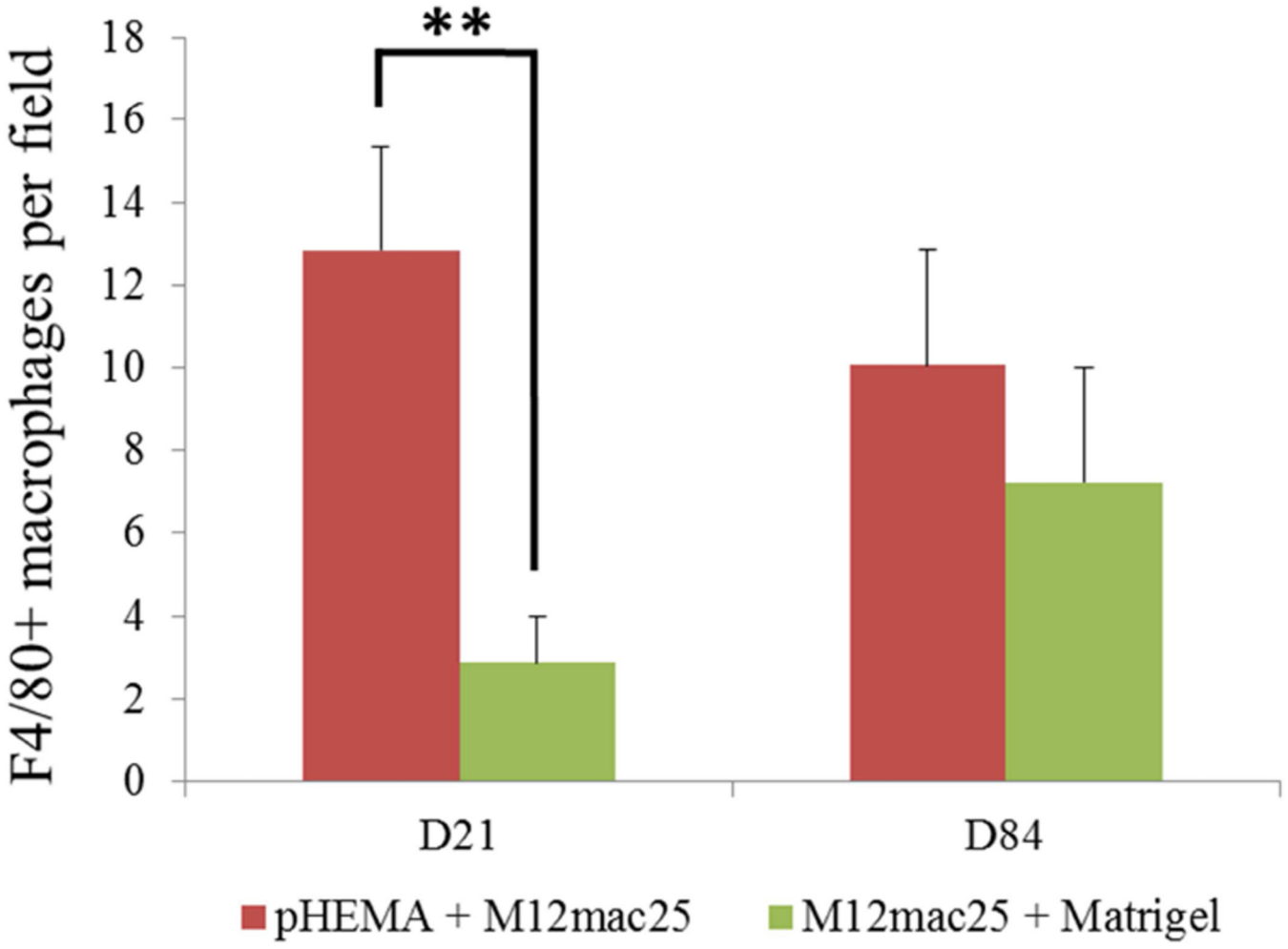

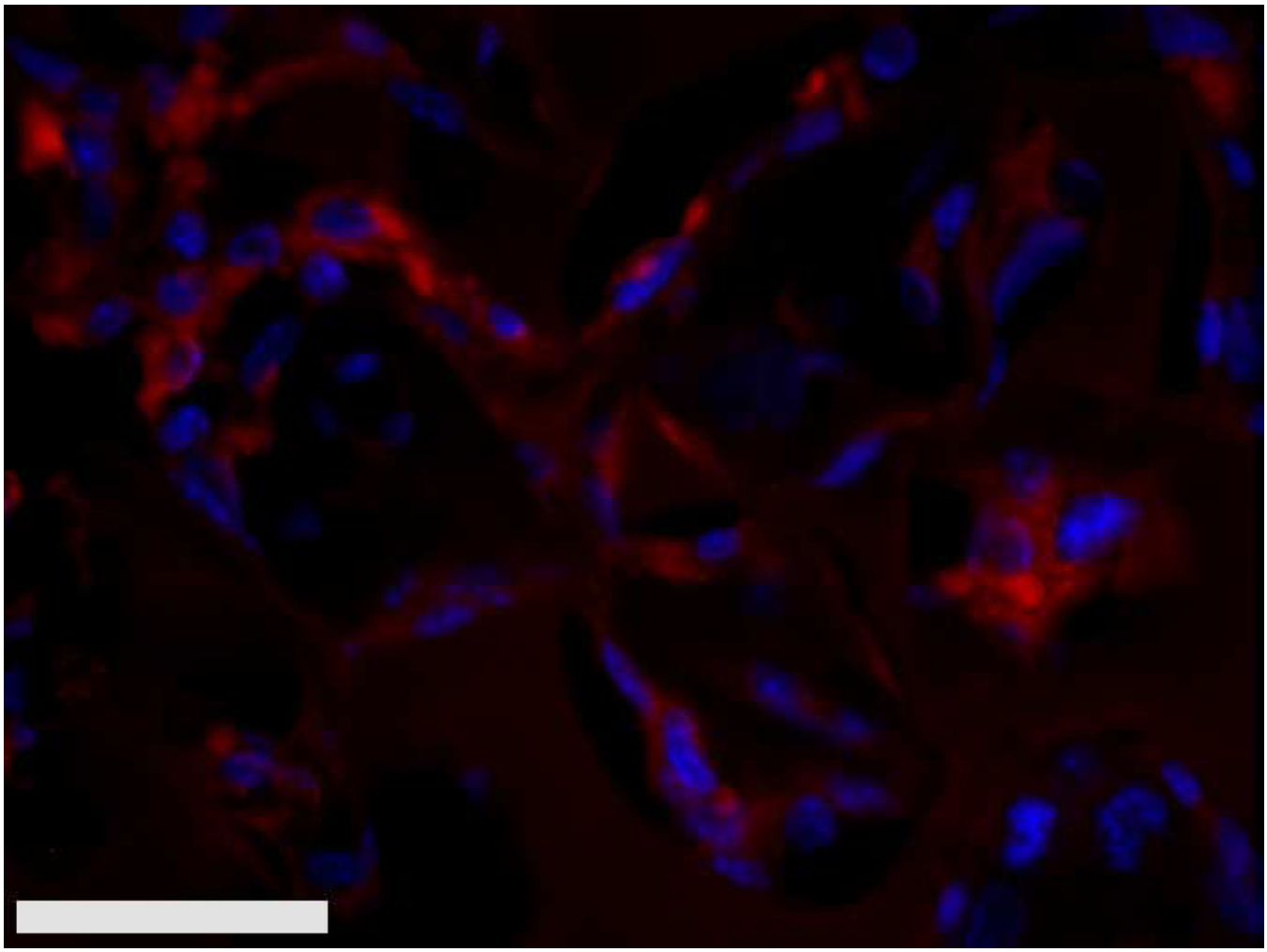

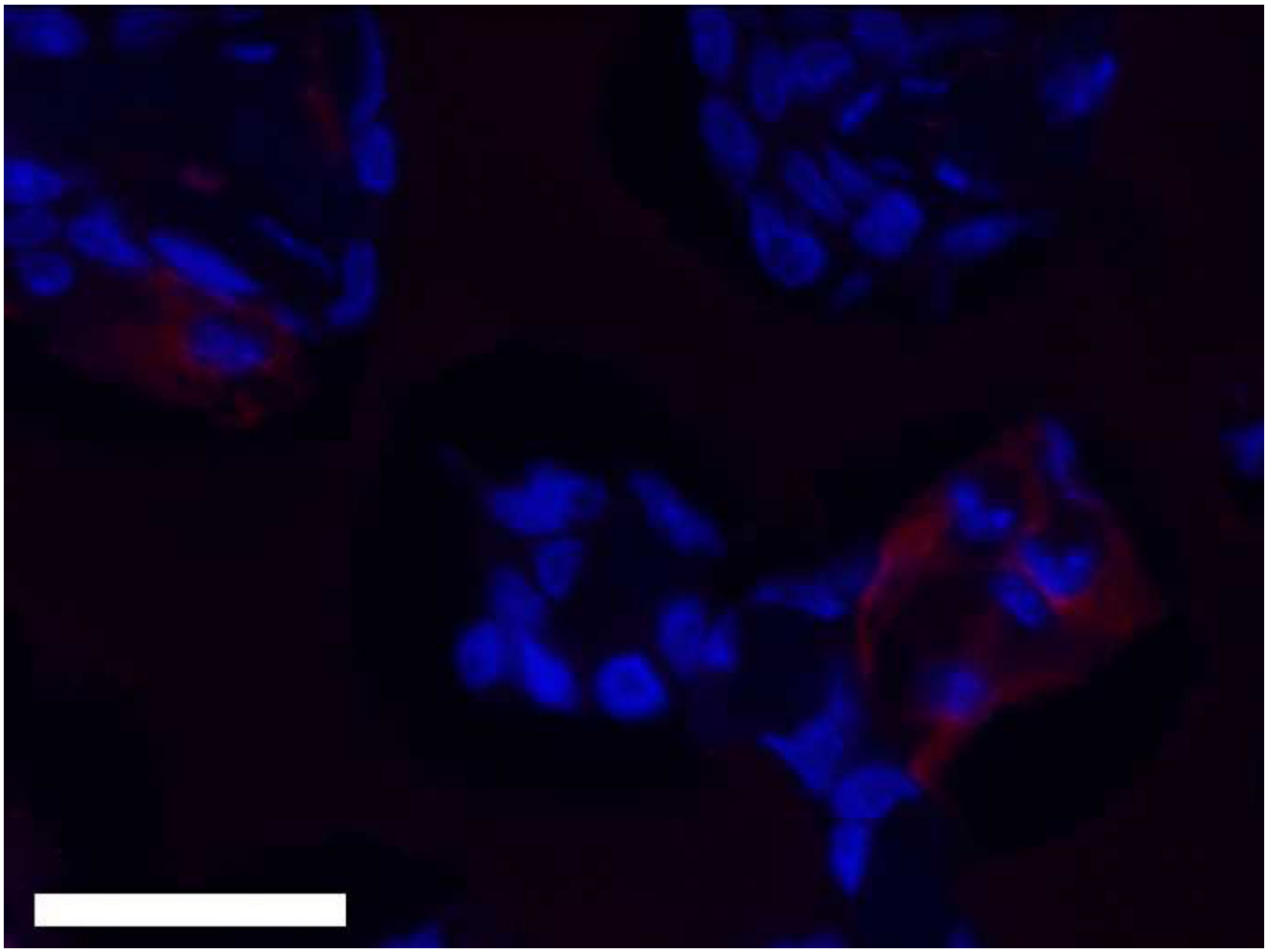

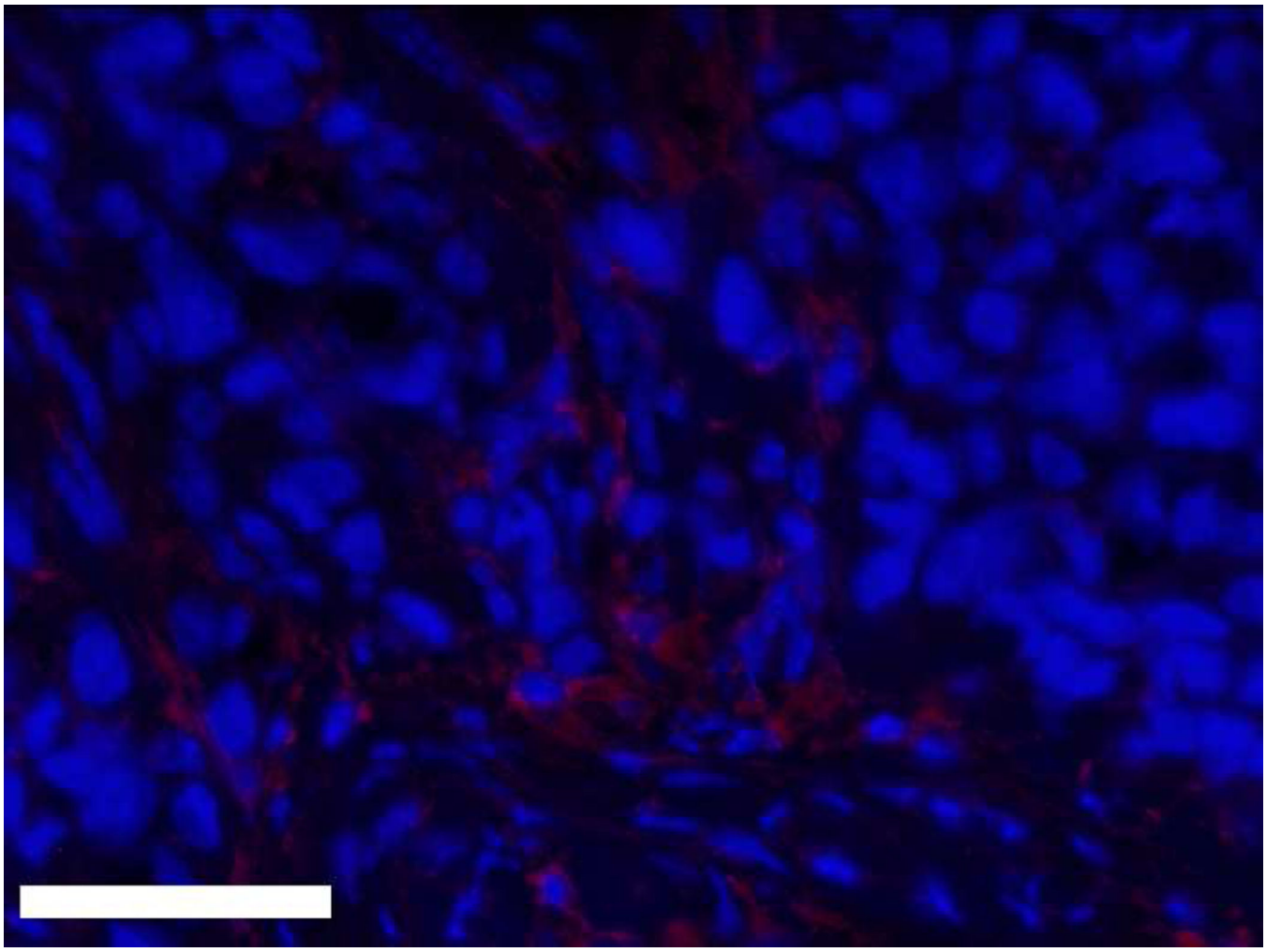

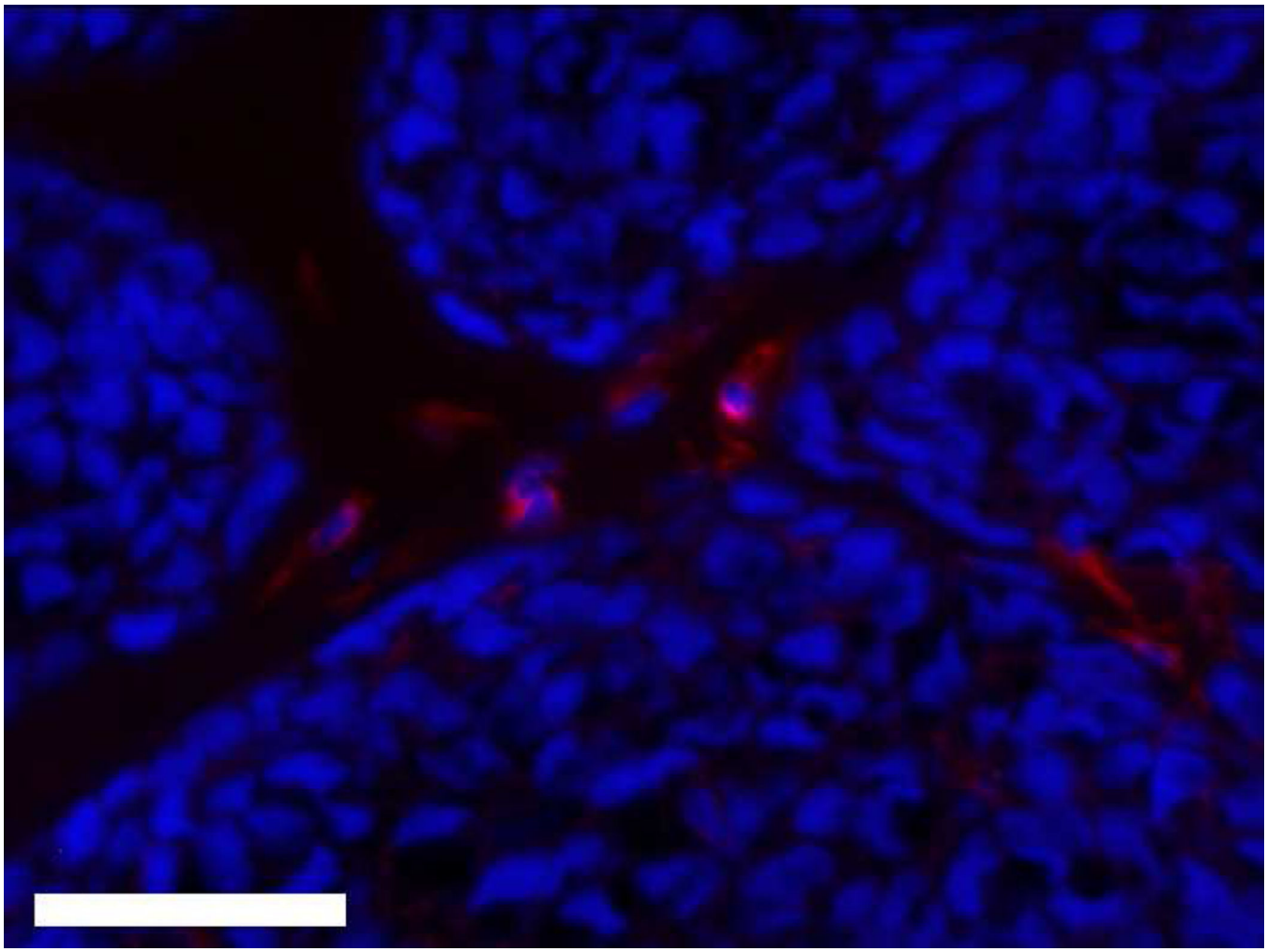

Figure 11.

(A) F4/80 macrophage staining of three week M12mac25 explants showed a significantly higher macrophage density in pHEMA-derived xenografts relative to those from Matrigel (** $p < 0.005$). The density remained higher at twelve weeks, though not significantly. Fluorescent F4/80 IHC showed (B) substantial macrophage infiltration (red) within the pHEMA scaffold at three weeks (C) macrophages still present within the pHEMA but at a lower density by twelve weeks, (D) macrophages present in the M12mac25 tumor region outside the scaffold in close proximity to other cells at twelve weeks, and (E) macrophages in the Matrigel explants remaining mostly confined to the regions around M12mac25 cell clusters (scale bars 20 μm).

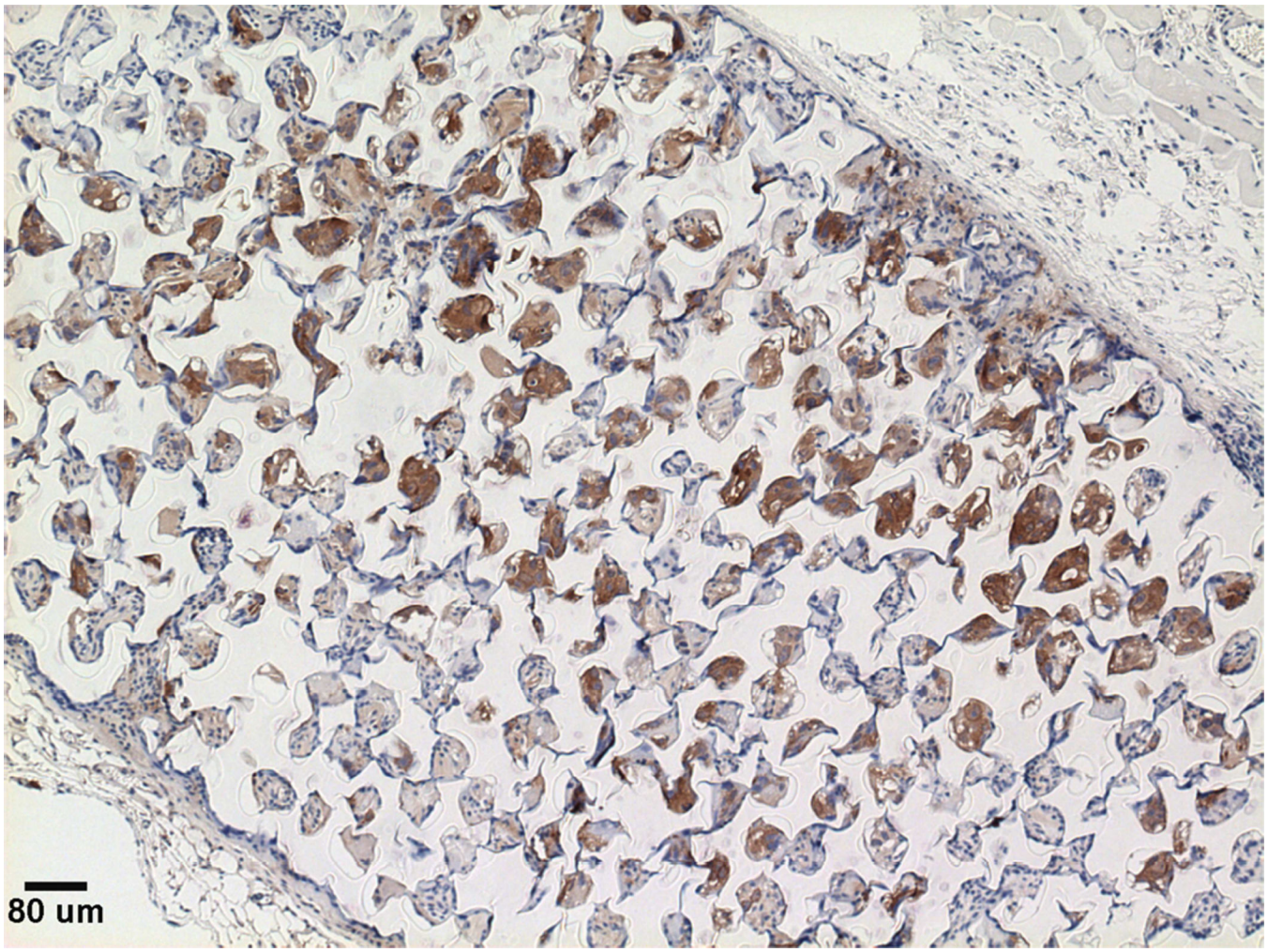

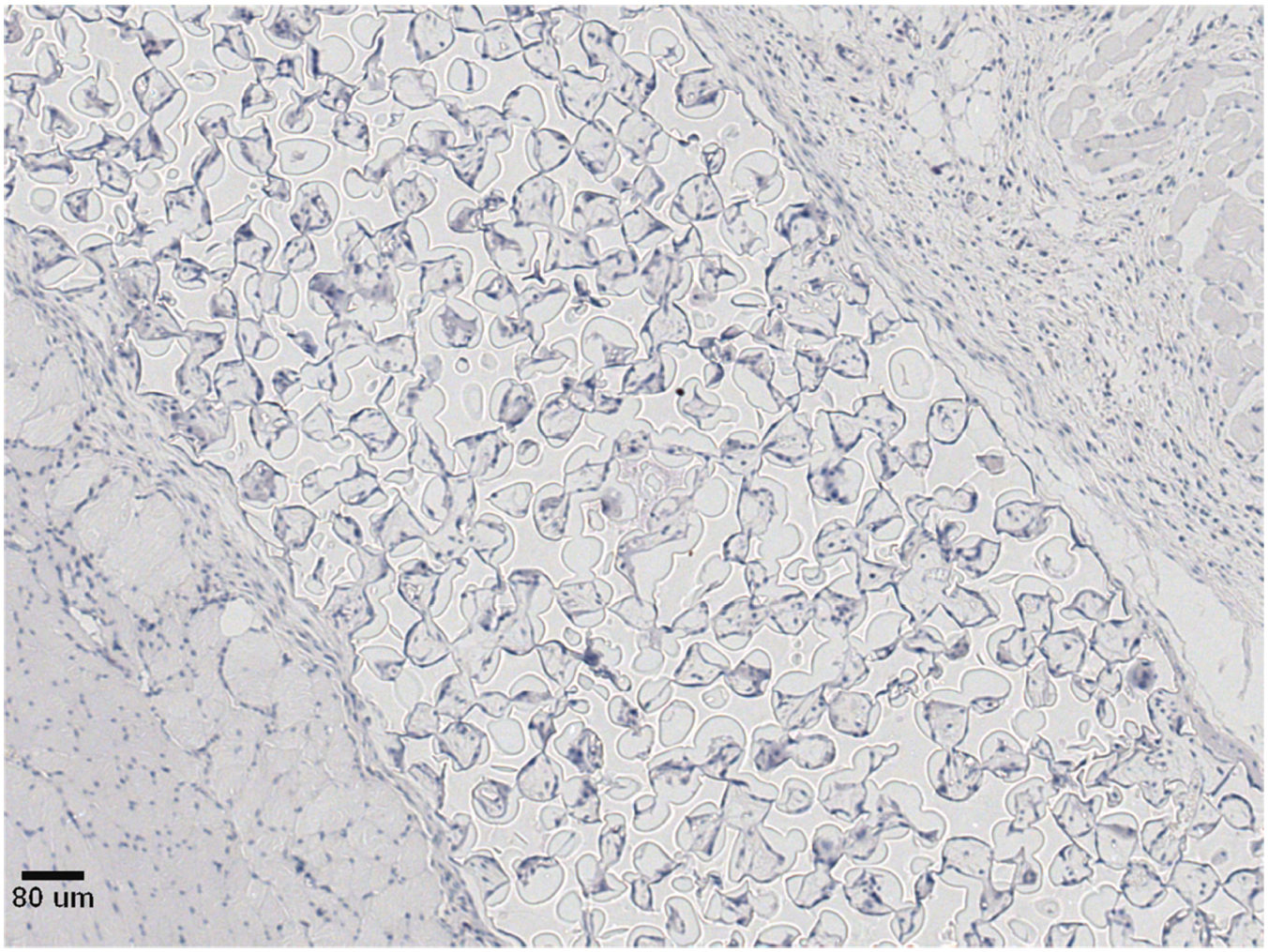

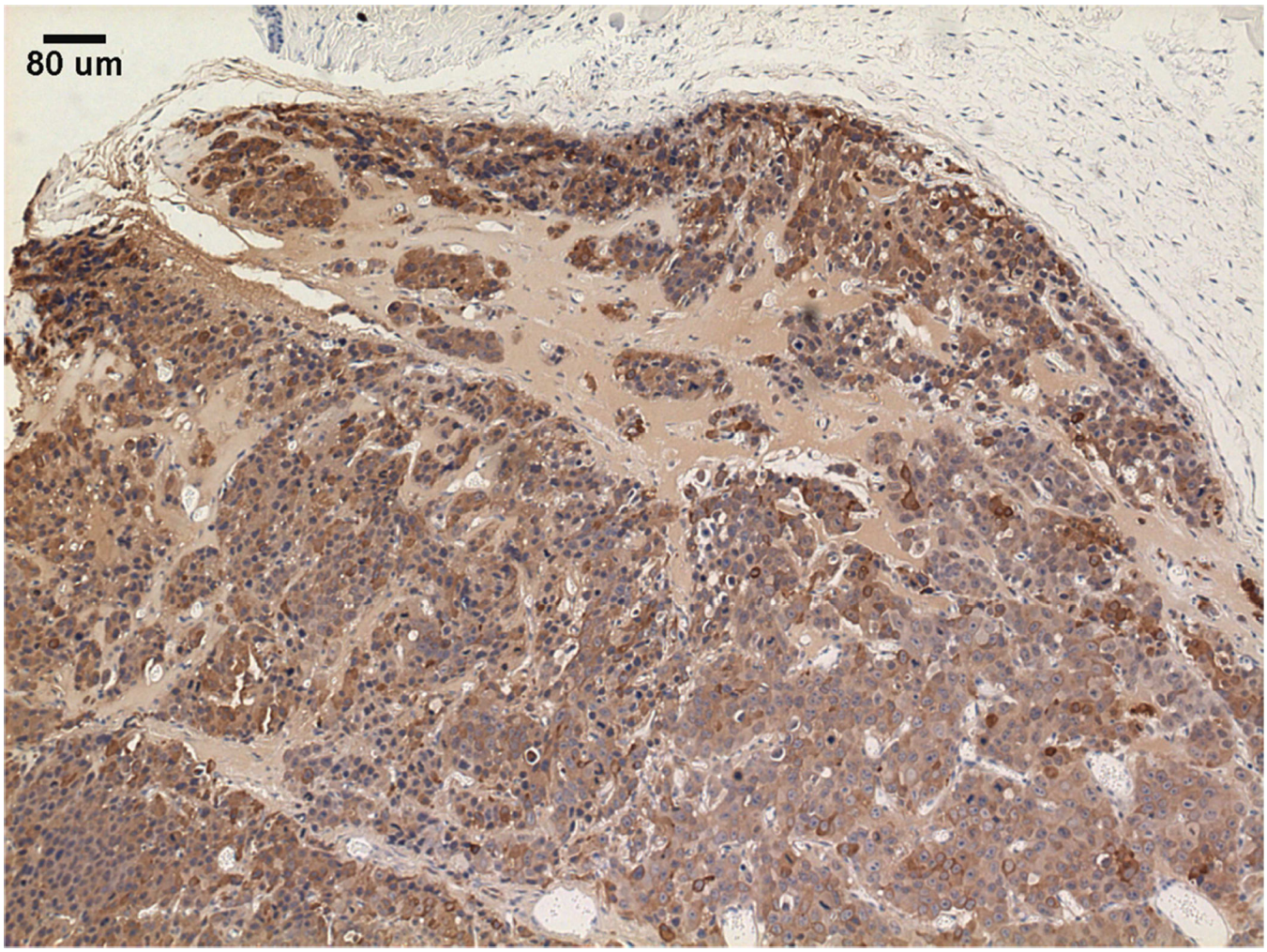

Figure 12.

PSA immunohistochemistry showing (A) a seven week pHEMA + LNCaP C4-2 explant with LNCaP cells contained within the scaffold without tumor growth, (B) a seven week pHEMA + LNCaP C4-2 explant with no remaining LNCaP C4-2 cells in the scaffold, and (C) a seven week LNCaP C4-2 + Matrigel xenograft staining strongly positive for PSA (scale bars 80 μm).